

Dynamical generation and transfer of nonclassical states in strongly interacting light-matter systems in cavities

Ilia Tutunnikov ¹, Vasil Rokaj ^{1,2,3,*}, Jianshu Cao ⁴ and H. R. Sadeghpour ¹

¹*ITAMP, Center for Astrophysics | Harvard & Smithsonian, Cambridge, Massachusetts 02138, USA*

²*Department of Physics, Villanova University, Villanova, Pennsylvania 19085, USA*

³*Department of Physics, Harvard University, Cambridge, Massachusetts 02138, USA*

⁴*Department of Chemistry, Massachusetts Institute of Technology, Cambridge, Massachusetts 02139, USA*

(Dated: October 3, 2024)

We propose leveraging strong and ultrastrong light-matter coupling to efficiently generate and exchange nonclassical light and quantum matter states. Two initial conditions are considered: (a) a displaced quadrature-squeezed matter state, and (b) a coherent state in a cavity. In both scenarios, polaritons mediate the dynamical generation and transfer of nonclassical states between light and matter. By monitoring the dynamics of both subsystems, we uncover the emergence of beatings in the collective matter oscillations. The beating period depends on the particle density through the vacuum Rabi splitting and peaks sharply under light-matter resonance conditions. For initial condition (a), nonclassicality is efficiently transferred from matter to photons under strong and ultrastrong coupling. However, for initial condition (b), nonclassical photonic states are generated only in the ultrastrong coupling regime due to the counter-rotating terms, highlighting the advantages of ultrastrong coupling. Furthermore, in the ultrastrong coupling regime, distinctive asymmetries relative to cavity detuning emerge in dynamical observables of both light and matter. The nonclassical photons can be extracted through a semi-transparent cavity mirror, while nonclassical matter states can be detected via time-resolved spectroscopy. This work highlights that hybrid polariton states can be utilized for dynamically generating nonclassical states, with potential applications in quantum state transfer.

I. INTRODUCTION

Strong light-matter coupling is essential for nascent quantum technologies, enabling efficient and reversible quantum state transfer. Polaritons, the light-matter quasiparticles, are often best manipulated in cavities [1–4], and have been widely studied in condensed matter [5–16], cold atoms [17–20], and molecular systems [21–31]. For example, polariton-based systems demonstrated modifications of chemical reactivity [21, 22, 30, 32–34], transient diffusivity and transport [28, 31, 35–42], as well as exciton-polariton condensation [17, 29, 43, 44].

Equally important is the ability to generate and manipulate photons in such hybrid polaritonic systems. Photon emission statistics has been explored in experiments with ultracold atomic gases, leveraging strong Rydberg correlations for deterministic single-photon generation [18, 19]. Second-order photon correlation measurements confirm the quantum nature of emitted light, achieving high fidelity with high-finesse optical cavities [45]. Squeezed light [46] has been demonstrated in various optomechanical systems [47, 48], e.g., mechanical resonators [49, 50], and ultracold atoms [51].

Here, we propose dynamically generating and transferring nonclassical states of quantum matter and light by leveraging strong light-matter coupling in a single-mode cavity [52, 53]. The model used to describe the composite-system dynamics is the archetypical Hopfield Hamiltonian (HH) [54], first introduced for studying excitonic response in dielectric crystals [54]. We show that the HH applies to various physical systems in cavities, including cold harmonically trapped ions [53], two-dimensional (2D) electron gases in a strong magnetic field (Landau levels) [5–8, 12, 15], and oriented polar molecules [55, 56].

Trapped ions are ideal for studying quantum phenomena, and ion-cavity systems have enabled single-photon emission, ion-photon, and ion-ion entanglement [57–60]. The position of a trapped ion can be precisely controlled within the cavity [61] and Fock, coherent, and squeezed motional states of a harmonically trapped

* vasil.rokaj@villanova.edu

ion have been generated [62]. Coherent transfer between an ion’s internal degrees of freedom and an optical cavity mode has been demonstrated in several experiments [63, 64]. In contrast, cavity coupling with the trapped ion motional states is technically more challenging due to the relatively low characteristic motional frequencies, often in the MHz range [60, 65].

Importantly, it has been shown that Landau levels exhibit ultrastrong coupling to the cavity field [3, 8–10, 12, 66–68] and Landau polariton states have been observed [7, 8, 12, 68–70]. More recently, mechanisms for cavity-induced modification of the integer Hall effect were proposed [71, 72], and the breakdown of topological protection has been experimentally demonstrated [5].

Further, recent experiments provide evidence that chemical reactions may be substantially affected by strong coupling between molecular vibrational modes and the electromagnetic modes of infrared (IR) microcavities—a phenomenon known as vibrational strong coupling (VSC) [30, 73–75]. This has led to extensive theoretical work [24, 40, 76–80] in elucidating the mechanism behind the observed effects. Typically, the rotational degrees of freedom introduce additional challenges for manipulating molecules. Nevertheless, there is rich literature on the coherent control of molecules, including techniques tailored to targeting vibrations [81, 82].

This work focuses on the collective dynamics in cavity quantum electrodynamics (QED) systems by considering two schemes to generate and transfer nonclassical states of light and matter in a cavity. In **Scheme I**, the matter state is displaced and quadrature-squeezed. The dynamics of both subsystems are monitored, and we uncover the emergence of beatings in the collective matter oscillations. The beating period depends on the detuning and peaks sharply around the light-matter resonance. This phenomenon highlights that collective dynamics of matter can be significantly modified via strong and resonant light-matter interaction in a cavity, even without an external field, i.e., in vacuum. Similar resonant modifications have been observed in chemical reactions in molecules under VSC [21, 22, 30, 32–34]. Looking into the photons, the cavity coupling *transfers* the quantum state of matter to light, resulting in sub-Poissonian photon number distribution (PND), i.e., quantum photonic states with no classical analogue [83]. In **Scheme II**, the cavity is initiated in a coherent state [84], which partially moves from one subsystem to another over time. Simultaneously, the counter-rotating light-matter interaction terms (counter-rotating terms, CRT) in the HH (see below) induce nonclassical features in light or matter subsystems depending on the initial shift of the coherent state. In the second scheme, the nonclassical features arise entirely from the CRT, underscoring the importance of the ultrastrong coupling [3, 85].

Notably, the CRT induce asymmetries in dynamical observables associated with the matter and light subsystems. These asymmetries emerge in the ultrastrong coupling regime when the cavity frequency is scanned around the resonance and are consequences of the asymmetry in the polaritonic branches. In contrast to linear spectral measurements, which may be insensitive to the quantum nature of the system, time-dependent observables involving higher-order moments of the matter or light distributions (e.g., photon number variance) serve as quantum measures sensitive to ultrastrong coupling effects. We provide analytical expressions for the average photon number in both schemes, allowing for a comprehensive description of photon generation over the entire parameter space, including the system parameters and initial state conditions.

We quantify the temporal evolution of nonclassical features in matter and light states using the time-averaged Mandel Q parameter for light and matter. For Scheme I, we demonstrate that outcoupling the cavity field through a semi-transparent cavity mirror allows for extracting the nonclassical photons [86]. In Scheme II applied to trapped ions, for instance, sideband spectroscopy of motional state population allows for the measurement of matter quantum state statistics [65]. Hybrid, polaritonic quantum systems can be utilized for the efficient transfer of nonclassicality from matter to light. Nonclassical states are necessary for sensing beyond the standard quantum limit [87–90], and likely for quantum information technologies [91, 92]. Our work bridges strong and ultrastrong light-matter coupled systems with quantum science and suggests novel pathways for polaritonic quantum technologies.

II. HOPFIELD HAMILTONIAN ACROSS DIFFERENT CAVITY QED SYSTEMS

In recent years, the HH has attracted significant attention due to its application in several cavity QED systems operating in the ultrastrong light-matter coupling regime [3, 85]. This section explicitly demonstrates how the HH emerges in three example systems in a cavity: cold trapped ions, 2D electron gas in a

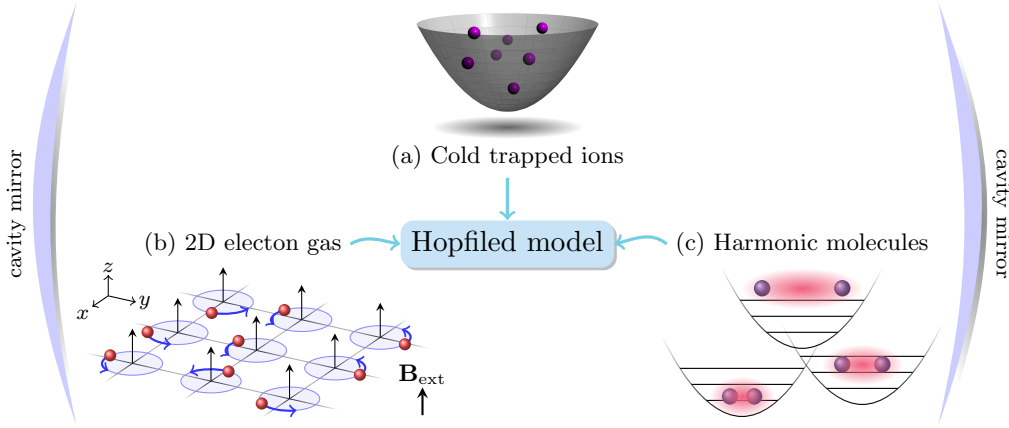


FIG. 1. Schematic illustration of the collective coupling to a homogeneous quantum cavity field in different physical systems, including (a) harmonically trapped cold ions, (b) 2D electron gas in a strong magnetic field, \mathbf{B}_{ext} , and (c) molecules with harmonic internuclear potential. In all cases, the system Hamiltonian can be mapped onto the HH, see Eqs. (5), (10), and (14). Thus, the dynamical phenomena described hereafter can be, in principle, realized in various cavity QED systems.

strong magnetic field, and oriented molecules with harmonic internuclear potential. Thus, in principle, the nonclassical dynamical phenomena discussed hereafter are within experimental reach across various physical systems.

A. Cold Trapped Ions

We start by considering a system of N interacting ions confined in a harmonic potential, coupled to a single-mode quantized cavity field [Fig. 1(a)]. Recently, this system was used to study the collective phenomena in the polaritonic ground state [53]. Here, we focus on the dynamics mediated by the coupling between the ions' motion and the cavity field. In the non-relativistic limit, this system is described by the Pauli-Fierz Hamiltonian in the Coulomb gauge, also known as the minimal-coupling Hamiltonian [56, 93]

$$\hat{H}_{\text{ion}} = \frac{1}{2m} \sum_{i=1}^N (i\hbar\nabla_i + g_0\hat{\mathbf{A}})^2 + \sum_{i<l}^N W(\hat{\mathbf{r}}_i - \hat{\mathbf{r}}_l) + \sum_{i=1}^N \frac{m\Omega^2}{2} \hat{\mathbf{r}}_i^2 + \sum_{\nu=x,y} \hbar\omega \left(\hat{a}_\nu^\dagger \hat{a}_\nu + \frac{1}{2} \right), \quad (1)$$

where g_0 is the single-particle coupling parameter to the cavity field (in units of the elementary charge, e), m is the mass of the particles, and Ω is the frequency of the harmonic trap. The quantized vector potential $\hat{\mathbf{A}}$ in the long-wavelength limit (homogeneous approximation) is given by [55, 56, 93]

$$\hat{\mathbf{A}} = \sum_{\nu=x,y} \sqrt{\frac{\hbar}{2\epsilon_0\mathcal{V}\omega}} \mathbf{e}_\nu (\hat{a}_\nu + \hat{a}_\nu^\dagger), \quad (2)$$

where $\omega = c|k_z|$ is the frequency in the quantization volume \mathcal{V} , with wavevector in the z direction, ϵ_0 is the vacuum permittivity, and $\nu = x, y$ denote the two transversal polarization directions [56, 93]. The operators \hat{a}_ν and \hat{a}_ν^\dagger are the annihilation and creation operators of the photon field obeying $[\hat{a}_\nu, \hat{a}_{\nu'}^\dagger] = \delta_{\nu\nu'}$.

Expanding the covariant kinetic energy shows that the homogeneous photon field couples to the total momentum of the particles, $\hat{\mathbf{A}} \cdot \sum_{i=1}^N \nabla_i$, implying *collective* coupling to the cavity field through the particles' center of mass (CM). Thus, we change variables to the CM position $\hat{\mathbf{R}} = N^{-1/2} \sum_{i=1}^N \hat{\mathbf{r}}_i$, and the relative positions $\hat{\mathbf{r}}_j = N^{-1/2}(\hat{\mathbf{r}}_1 - \hat{\mathbf{r}}_j)$ ($j > 1$). The prefactor $N^{-1/2}$ is introduced for mathematical convenience like in [94]. The operators $\hat{\mathbf{R}}$ and $\hat{\mathbf{r}}_j$, along with their corresponding momenta commute. This confirms the independence of CM and relative coordinates (App. A 1).

The scalar trapping potential separates into two parts: the first one depends on the CM coordinate, while the second depends on the relative coordinates, without cross-terms between the two, $\sum_{i=1}^N \hat{\mathbf{r}}_i^2 =$

$\hat{\mathbf{R}}^2 + N \sum_{j=2}^N \hat{\mathbf{r}}_j^2 - (\sum_{j=2}^N \hat{\mathbf{r}}_j)^2$. The two-body interaction $W(\hat{\mathbf{r}}_i - \hat{\mathbf{r}}_l)$ depends only on the relative distances, so it does not affect the cavity-induced CM motion. The Hamiltonian, therefore, splits into two parts: (i) $\hat{H}_{\text{ion-cm}}$, describing the the CM coupling to the quantized field $\hat{\mathbf{A}}$, and (ii) $\hat{H}_{\text{ion-rel}}$, describing the dynamics of the relative coordinates, decoupled from both $\hat{\mathbf{A}}$ and the CM. Then,

$$\hat{H}_{\text{ion-cm}} = \frac{1}{2m} (i\hbar\nabla_{\mathbf{R}} + g_0\sqrt{N}\hat{\mathbf{A}})^2 + \frac{m\Omega^2}{2}\hat{\mathbf{R}}^2 + \sum_{\nu=x,y} \hbar\omega \left(\hat{a}_\nu^\dagger \hat{a}_\nu + \frac{1}{2} \right), \quad (3)$$

and $\hat{H}_{\text{ion-rel}}$ is presented in App. A 1.

We now focus exclusively on the CM part to describe the cavity-matter dynamics. Since the polarization vectors of the photon field lie in the (x, y) plane, the z direction is trivial. The light-matter Hamiltonian then becomes a system of interacting harmonic oscillators, and importantly, the x and y directions are decoupled,

$$\hat{H}_{\text{ion-cm}} = \sum_{\nu=x,y} \left[-\frac{\hbar^2}{2m} \partial_{R_\nu}^2 + \frac{ig_0\hbar}{m} \sqrt{N} \hat{A}_\nu \partial_{R_\nu} + \frac{m\Omega^2}{2} \hat{R}_\nu^2 + \frac{Ng_0^2}{2m} \hat{A}_\nu^2 + \hbar\omega \left(\hat{a}_\nu^\dagger \hat{a}_\nu + \frac{1}{2} \right) \right]. \quad (4)$$

To avoid any confusion, note that $\hat{\mathbf{R}} = (\hat{R}_x, \hat{R}_y) = (\hat{X}, \hat{Y})$, $\nabla_{\hat{\mathbf{R}}} = (\partial_{R_x}, \partial_{R_y}) = (\partial_X, \partial_Y)$ and $\hat{\mathbf{A}} = (\hat{A}_x, \hat{A}_y)$. Consequently, without loss of generality, we can focus only on the X component of the Hamiltonian. We also suppress the x index in the photon operators for simplicity, i.e., $\hat{a} \equiv \hat{a}_x$. Finally, to simplify the Hamiltonian, we introduce bosonic operators for matter $\hat{b} = \sqrt{m\Omega/(2\hbar)}[\hat{X} + \hbar/(m\Omega)\partial_X]$. The CM Hamiltonian turns into the well-known HH [54, 85]

$$\hat{H}_{\text{ion-cm}} = \hbar\omega \left(\hat{b}^\dagger \hat{b} + \frac{1}{2} \right) + i\hbar \sqrt{\frac{\Omega g_0^2 N}{4m\epsilon_0 \mathcal{V} \omega}} (\hat{a} + \hat{a}^\dagger) (\hat{b} - \hat{b}^\dagger) + \frac{\hbar N g_0^2}{4m\epsilon_0 \mathcal{V} \omega} (\hat{a} + \hat{a}^\dagger)^2 + \hbar\omega \left(\hat{a}^\dagger \hat{a} + \frac{1}{2} \right). \quad (5)$$

B. 2D Electron Gas

Next, we consider 2D electron gas (2deg) subject to a homogeneous magnetic field perpendicular to the plane. The electrons are coupled to a homogeneous single-mode cavity field [Fig. 1(b)]. Landau-level systems in a cavity have been theoretically studied [7, 15], and, notably, have been experimentally realized. Many interesting phenomena have been observed, including Landau polariton quasiparticles and modifications of quantum Hall transport [5, 6, 8, 12]. The Hamiltonian for the quantum Hall system in the cavity is given by

$$\hat{H}_{2\text{deg}} = \frac{1}{2m} \sum_{i=1}^N (\hat{\boldsymbol{\pi}}_i + e\hat{\mathbf{A}})^2 + \sum_{i<l}^N W(\hat{\mathbf{r}}_i - \hat{\mathbf{r}}_l) + \hbar\omega \left(\hat{a}^\dagger \hat{a} + \frac{1}{2} \right), \quad (6)$$

where $\hat{\boldsymbol{\pi}}_i = i\hbar\nabla_i + e\hat{\mathbf{A}}_{\text{ext}}(\hat{\mathbf{r}}_i)$ are the dynamical momenta, and $\hat{\mathbf{A}}_{\text{ext}}(\hat{\mathbf{r}}) = -\mathbf{e}_y B \hat{x}$ describes the magnetic field $\hat{\mathbf{B}} = \nabla \times \hat{\mathbf{A}}_{\text{ext}}(\hat{\mathbf{r}}) = B\mathbf{e}_z$. The cavity field $\hat{\mathbf{A}} = \sqrt{\hbar/(2\epsilon_0 \mathcal{V} \omega)} \mathbf{e}_y (\hat{a} + \hat{a}^\dagger)$ is characterized by the in-plane polarization vector \mathbf{e}_x and the photon's bare frequency ω . Further, $W(\hat{\mathbf{r}}_i - \hat{\mathbf{r}}_j) = (4\pi\epsilon_0)^{-1} |\hat{\mathbf{r}}_i - \hat{\mathbf{r}}_j|$ is the Coulomb interaction between the electrons. The transformations of momenta $\{\nabla_i\}$ and the two-body interaction are described in App. A 1.

The interaction between the cavity field and the electrons is given by $\hat{\mathbf{A}} \cdot \sum_{i=1}^N i\hbar\nabla_i + e\hat{\mathbf{A}}_{\text{ext}}(\hat{\mathbf{r}}_i) = \sqrt{N}\hat{\mathbf{A}} \cdot [i\hbar\nabla_{\mathbf{R}} + e\hat{\mathbf{A}}_{\text{ext}}(\hat{\mathbf{R}})]$, such that the cavity field couples only to the CM of the 2deg (App. A 2). The Hamiltonian in the new frame, $\hat{H}_{2\text{deg}} = \hat{H}_{2\text{deg-cm}} + \hat{H}_{2\text{deg-rel}}$ is a sum of (i) the CM part, $\hat{H}_{2\text{deg-cm}}$ including the coupling to the quantized field $\hat{\mathbf{A}}$, and (ii) $\hat{H}_{2\text{deg-rel}}$ depending on the relative distances and decoupled from $\hat{\mathbf{A}}$. The CM part, governing the light-matter dynamics, is given by

$$\hat{H}_{2\text{deg-cm}} = \frac{1}{2m} \left(i\hbar\nabla_{\mathbf{R}} + e\hat{\mathbf{A}}_{\text{ext}}(\hat{\mathbf{R}}) + e\sqrt{N}\hat{\mathbf{A}} \right)^2 + \hbar\omega \left(\hat{a}^\dagger \hat{a} + \frac{1}{2} \right). \quad (7)$$

The expression for $\hat{H}_{2\text{deg-rel}}$ is presented in the App. A 2. In the Landau gauge, the Hamiltonian is translationally invariant along the y axis. This implies that the eigenfunctions related to this direction in space

are plane waves $\exp(iK_y\hat{Y})$. Applying $\hat{H}_{2\text{deg-cm}}$ to the plane wave and introducing the shifted coordinate $\hat{X} = \hat{X} + \hbar K_y/eB$, the Hamiltonian becomes

$$\hat{H}_{2\text{deg-cm}} = -\frac{\hbar^2}{2m} \frac{\partial^2}{\partial \hat{X}^2} + \frac{m\omega_c^2}{2} \hat{X}^2 - \frac{e^2 B \sqrt{N}}{m} \hat{A} \hat{X} + \frac{e^2 N \hat{A}^2}{2m} + \hbar\omega \left(\hat{a}^\dagger \hat{a} + \frac{1}{2} \right). \quad (8)$$

To simplify the Hamiltonian further, we perform a Fourier transformation on the electronic coordinate $\phi(\hat{X}) = (2\pi)^{-1} \int_{-\infty}^{\infty} \tilde{\phi}(\hat{K}) \exp(-i\hat{K}\hat{X}) d\hat{K}$, such that

$$\hat{H}_{2\text{deg-cm}} = -\frac{m\omega_c^2}{2} \frac{\partial^2}{\partial \hat{K}^2} + \frac{\hbar^2}{2m} \hat{K}^2 + i \frac{e^2 B \sqrt{N}}{m} \hat{A} \partial_K + \frac{e^2 N \hat{A}^2}{2m} + \hbar\omega \left(\hat{a}^\dagger \hat{a} + \frac{1}{2} \right). \quad (9)$$

Finally, to turn the Hamiltonian into HH, we introduce annihilation and creation operators $\{\hat{l}, \hat{l}^\dagger\}$ for the matter degrees of freedom $\hat{K} = \sqrt{m\omega_c/(2\hbar)}(\hat{l} + \hat{l}^\dagger)$ and $\partial_K = \sqrt{\hbar/(2m\omega_c)}(\hat{l} - \hat{l}^\dagger)$, such that

$$\hat{H}_{2\text{deg-cm}} = \hbar\omega_c \left(\hat{l}^\dagger \hat{l} + \frac{1}{2} \right) + i\hbar \sqrt{\frac{e^2 N \omega_c}{4m\epsilon_0 \mathcal{V} \omega}} (\hat{a} + \hat{a}^\dagger)(\hat{l} - \hat{l}^\dagger) + \frac{\hbar e^2 N}{4m\epsilon_0 \mathcal{V} \omega} (\hat{a} + \hat{a}^\dagger)^2 + \hbar\omega \left(\hat{a}^\dagger \hat{a} + \frac{1}{2} \right). \quad (10)$$

Thus, the CM Hamiltonian for Landau levels coupled to the cavity assumes the same mathematical form as that of harmonically trapped ions, with one important difference. To obtain Eq. (10), we applied a Fourier transformation on the matter operators. As a result, the dynamical phenomena that occur in real space for the ions manifest in k -space for the Landau levels.

C. Harmonic Molecules

As another example, consider a system of N identical non-interacting polar molecules collectively coupled to a single-mode cavity. The molecular vibrations are described by one-dimensional harmonic potential. For simplicity, the molecules are considered oriented along one of the cavity polarization directions. For the molecular system, we use the length gauge form of the Pauli-Fierz Hamiltonian [55, 56], which, given these assumptions, takes the form

$$\hat{H}_{\text{mol}} = \sum_{i=1}^N \left[-\frac{\hbar^2}{2M} \frac{\partial^2}{\partial x_i^2} + \frac{M\Omega_{\text{vib}}^2 \hat{x}_i^2}{2} \right] + \hbar\omega \left[-\frac{1}{2} \frac{\partial^2}{\partial q^2} + \frac{1}{2} \left(\hat{q} - g \sum_{i=1}^N \hat{x}_i \right)^2 \right]. \quad (11)$$

Here, Ω_{vib} is the fundamental frequency of the harmonic potential, M is the mass of the molecule, and ω is the cavity frequency. $g = \mu_0/\sqrt{\omega\epsilon_0\mathcal{V}}$ is the dimensionless light-molecule coupling constant, which depends on the effective cavity volume \mathcal{V} , the vacuum permittivity ϵ_0 , and the magnitude of the molecular dipole moment, μ_0 . The operators \hat{q} and ∂_q describe the position and momentum quadratures of the bosonic cavity mode. However, they should not be confused with the creation and annihilation photon operators \hat{a}^\dagger, \hat{a} in the Coulomb gauge, as their connection is subtle [95].

The model Hamiltonian \hat{H}_{mol} has been used in multiple works studying molecular systems under vibrational strong coupling in cavities [24, 77–80]. The perfectly oriented molecules couple to the cavity through the collective dipole moment. Thus, we transform \hat{H}_{mol} into the CM frame by introducing the CM coordinate $\hat{X} = (N)^{-1/2} \sum_i \hat{x}_i$ and the relative bond lengths $\hat{x}_j = (\hat{x}_1 - \hat{x}_j)/\sqrt{N}$ with $j > 1$. We already showed how the kinetic energy terms and the harmonic potential transform into the CM frame in App. A 1. Thus, it is straightforward to obtain the CM Hamiltonian, while the relative lengths Hamiltonian separates like in the previous models,

$$\begin{aligned} \hat{H}_{\text{mol-cm}} &= -\frac{\hbar^2}{2M} \frac{\partial^2}{\partial \hat{X}^2} + \frac{M\Omega_{\text{vib}}^2}{2} \hat{X}^2 + \hbar\omega \left[-\frac{1}{2} \frac{\partial^2}{\partial q^2} + \frac{1}{2} \left(\hat{q} - g\sqrt{N}\hat{X} \right)^2 \right], \\ \hat{H}_{\text{mol-rel}} &= \frac{1}{2m} \sum_{j=2}^N \left(\frac{i\hbar}{\sqrt{N}} \partial_{\hat{x}_j} \right)^2 - \frac{\hbar^2}{2mN} \sum_{j,k=2}^N \partial_{\hat{x}_j} \cdot \partial_{\hat{x}_k} + \frac{m\Omega^2}{2} N \sum_{j=2}^N \hat{x}_j^2 - \frac{m\Omega^2}{2} \left[\sum_{j=2}^N \hat{x}_j \right]^2. \end{aligned} \quad (12)$$

The cavity mode quadrature, \hat{q} , couples only to the CM coordinate \hat{X} in $\hat{H}_{\text{mol-cm}}$. We next expand $(\hat{q} - g\sqrt{N}\hat{X})^2$ and apply Fourier transformation to \hat{q} , $\phi(\hat{q}) = (2\pi)^{-1} \int_{-\infty}^{\infty} \tilde{\phi}(\hat{p}) \exp(i\hat{p}\hat{q}) d\hat{p}$. We find that the cavity-molecules CM Hamiltonian has the same mathematical form as the previously discussed two models,

$$\hat{H}_{\text{mol-cm}} = -\frac{\hbar^2}{2M} \frac{\partial^2}{\partial X^2} + \frac{M\Omega_{\text{vib}}^2}{2} \hat{X}^2 + \frac{\hbar\omega g^2 N}{2} \hat{X}^2 + i\hbar\omega g\sqrt{N}\hat{X} \frac{\partial}{\partial p} + \hbar\omega \left(-\frac{1}{2} \frac{\partial^2}{\partial p^2} + \frac{\hat{p}^2}{2} \right). \quad (13)$$

Finally, we can write the above Hamiltonian in terms of annihilation and creation operators, $\hat{m} = \sqrt{M\Omega_{\text{vib}}}/(2\hbar)[\hat{X} + \hbar/(M\Omega_{\text{vib}})\partial_X]$ for matter, and $\hat{c} = (\hat{p} + \partial_p)/\sqrt{2}$ for light,

$$\hat{H}_{\text{mol-cm}} = \hbar\Omega_{\text{vib}} \left(\hat{m}^\dagger \hat{m} + \frac{1}{2} \right) + i\hbar\omega g \sqrt{\frac{\hbar N}{4M\Omega_{\text{vib}}}} (\hat{m}^\dagger + \hat{m})(\hat{c} - \hat{c}^\dagger) + \frac{\hbar^2\omega g^2 N}{4M\Omega_{\text{vib}}} (\hat{m}^\dagger + \hat{m})^2 + \hbar\omega \left(\hat{c}^\dagger \hat{c} + \frac{1}{2} \right). \quad (14)$$

The molecule-cavity Hamiltonian above has the standard form of the HH [54]. However, the bosonic quadratic term shows up for the matter operators \hat{m} , \hat{m}^\dagger . Thus, the dynamics that appear for photons in the ion-cavity system will manifest for the matter in the molecule-cavity system.

D. Hopfield Hamiltonian for the Center of Mass and Polariton Modes

In the previous subsections, we demonstrated that, across three cavity QED platforms, the collective coupling of an ensemble of particles (ions, 2degs, molecules) is described by the HH in Eq. (5). In all cases, the bosonic/harmonic matter part is given by $\sim \hbar\Omega\hat{b}^\dagger\hat{b}$, the cavity mode is described by $\sim \hbar\omega\hat{a}^\dagger\hat{a}$, the bilinear interaction is $\sim \sqrt{N}(\hat{a} + \hat{a}^\dagger)(\hat{b} - \hat{b}^\dagger)$. The last term is the quadratic photon self-interaction in the Coulomb gauge, $\sim N(\hat{a} + \hat{a}^\dagger)^2$, or the matter self-interaction, $\sim N(\hat{m} + \hat{m}^\dagger)^2$, in the length gauge.

In what follows, we examine the dynamics of the HH, focusing on trapped ions for concreteness, as this system is more intuitive than 2D electron gas (Landau levels) or molecules. We assume the cavity consists of two flat parallel mirrors with area \mathcal{A} , separated by a distance L , giving an effective cavity volume $\mathcal{V} = \mathcal{A}L$. From this, the dimensionless form of Eq. (5) is given by

$$\hat{\mathcal{H}} = \frac{1}{2}(\hat{P}^2 + \hat{X}^2) + \frac{\gamma}{2}(\hat{p}^2 + \hat{q}^2) - \lambda\hat{q}\hat{P} + \frac{\lambda^2}{2}\hat{q}^2, \quad (15)$$

where $\hat{X} \equiv (\hat{b}^\dagger + \hat{b})/\sqrt{2}$ and $\hat{P} \equiv i(\hat{b}^\dagger - \hat{b})/\sqrt{2}$ are the CM position and momentum operators (\hat{b}^\dagger and \hat{b} are the corresponding creation and annihilation operators), $\hat{q} \equiv (\hat{a}^\dagger + \hat{a})/\sqrt{2}$, $\hat{p} \equiv i(\hat{a}^\dagger - \hat{a})/\sqrt{2}$ represent the position and momentum field quadratures. Energy, time, length, and momentum are measured in units of $\hbar\Omega$, $1/\Omega$, $\sqrt{\hbar/(m\Omega)}$, and $\sqrt{\hbar m\Omega}$, respectively. The field quadratures associated with position and momentum are measured in units of $\sqrt{\hbar/(\epsilon_0 V\Omega)}$ and $\sqrt{\hbar\epsilon_0 V\Omega}$, respectively. The two dimensionless control parameters of $\hat{\mathcal{H}}$ are the frequency ratio between the cavity and the CM matter excitations, γ , and the collective coupling constant, λ , defined as [53]

$$\gamma \equiv \frac{\omega}{\Omega}, \quad \lambda \equiv \sqrt{\frac{Ng_0^2}{\pi\epsilon_0 c\mathcal{A}m\Omega}}. \quad (16)$$

The two polariton branches have energies Ω_\pm , given by [53]

$$\Omega_\pm^2 = \frac{1 + \gamma^2 + \gamma\lambda^2}{2} \pm \frac{1}{2}\sqrt{(1 + \gamma^2 + \gamma\lambda^2)^2 - 4\gamma^2}. \quad (17)$$

The cavity resonates with the CM matter excitations at $\gamma = 1$. App. B shows the λ, γ -dependence of Ω_\pm .

We numerically solve the time-dependent Schrödinger equation with $\hat{\mathcal{H}}$ to study the light-matter dynamics. We also employ a semi-classical analysis to derive exact analytical expressions for the observables. This approach relies on solving Hamilton's equations of motion, derived from the classical equivalent of $\hat{\mathcal{H}}$, for $X(t)$, $P(t)$, $q(t)$, and $p(t)$, and provides further insight into the underlying dynamics of the coupled system (App. C). According to the Ehrenfest theorem, in a harmonic system, the first moments (e.g., $\langle \hat{X}(t) \rangle$, $\langle \hat{q}(t) \rangle$, etc.) match the corresponding classical solutions exactly [96, 97]. Position-momentum uncertainty manifests in higher-order observables (e.g., $\langle \hat{X}^2 \rangle$, $\langle \hat{P}^2 \rangle$, $\langle \hat{q}^2 \rangle$, etc.). These observables are obtained by averaging classical expressions over the initial phase space distribution, corresponding to the composite system initial wave function. The Mandel Q functions of matter or light, which quantify deviations from classically, are obtained using fully quantum simulations.

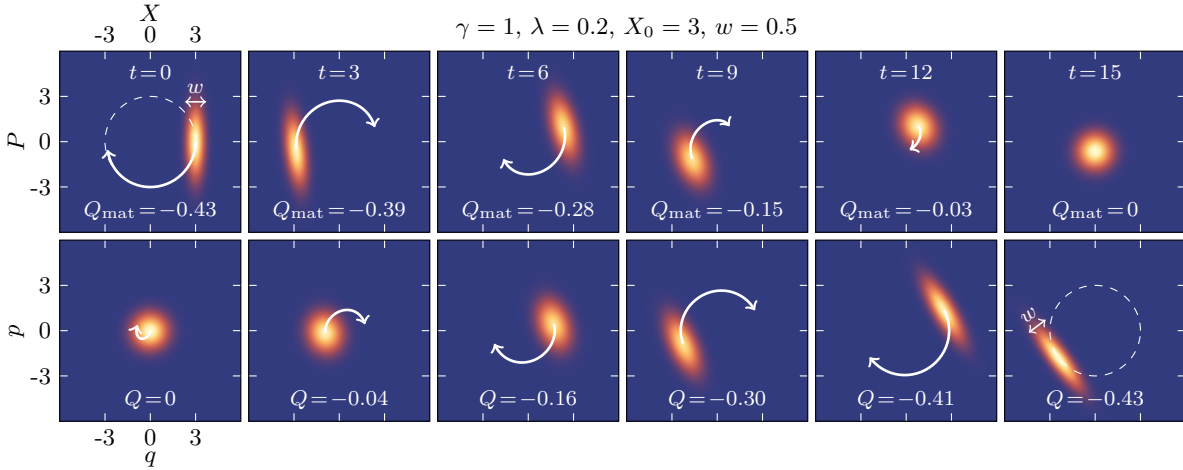


FIG. 2. Snapshots of time evolution of the matter (X, P , upper row) and cavity states (q, p , bottom row) in their respective phase spaces. The initial state in Scheme I is a product of a displaced quadrature-squeezed matter CM state and cavity ground state [see Eq. (18)]. Arrows indicate the trajectories of the phase space distribution centers. Initially, the radius of the trajectory equals the initial matter CM quadrature shift, X_0 . The dimensional units for the variables and parameters in this work are defined after Eq. (15).

III. SCHEME I. TRANSFER OF NONCLASSICALITY FROM MATTER TO LIGHT

The transfer of nonclassical states is demonstrated by initializing the composite system with the matter CM displaced by X_0 and quadrature-squeezed in X , while the cavity is in the vacuum state. The initial wave function of the composite system is given by $\psi_0(X, q) \propto \exp[-(X - X_0)^2/(2w^2)] \exp(-q^2/2)$, where w is the width of the matter wave function. For $w = 1$, the matter is in its ground state, and for $w < 1$, it is quadrature-squeezed. The wave function ψ_0 corresponds to the semi-classical phase space distribution

$$\mathcal{P}(0) = \frac{1}{\pi^2} e^{-[X(0)-X_0]^2 w^{-2} - P^2(0) w^2} e^{-q^2(0) - p^2(0)}, \quad (18)$$

with $X(0)$, $P(0)$, $q(0)$, and $p(0)$ representing the initial conditions. Fig. 2 presents a sequence of phase space snapshots for the light and matter subsystems. The initial state parameters are $X_0 = 3$ and $w = 0.5$, with light and matter at resonance ($\gamma = 1$), in the ultrastrong coupling regime ($\lambda = 0.2$).

On short timescales, the squeezed matter phase space distribution rotates counterclockwise at a radial distance of approximately X_0 while maintaining its elongated shape. As time progresses, the distribution becomes circularly symmetric and converges toward the origin. The motion of the phase space distribution has two characteristic frequencies defined by the polariton energies in Eq. (17): fast angular (or rotational) frequency, proportional to $\Omega_+ + \Omega_-$, and slow radial oscillation frequency, proportional to the vacuum Rabi splitting (VRS) $\bar{\Delta} \equiv \Omega_+ - \Omega_-$.

The matter CM dynamics, mediated by the light-matter coupling, generates photons and the nonclassical state of matter effectively transfers to the light on the time scale of slow radial oscillation ($\bar{\Delta}^{-1}$), as illustrated in the bottom row in Fig. 2. The light distribution shifts away from the origin and becomes squeezed, mirroring the initial state of the matter. At resonance, a complete transfer does not require ultrastrong light-matter interaction, but the transfer rate is defined by the coupling strength, $\bar{\Delta} = \lambda$.

More generally, the phase space distributions here are multivariate Gaussians, appearing as rotated ellipses centered around $(\langle \hat{X}(t) \rangle, \langle \hat{P}(t) \rangle)$ or $(\langle \hat{q}(t) \rangle, \langle \hat{p}(t) \rangle)$. The eigenvectors of the covariance matrix define the orientation of the ellipses while the aspect ratio is proportional to the ratio of the eigenvalues (App. D).

The Mandel Q function measures the deviation of PND from the Poisson distribution and is defined as [83]

$$Q \equiv \frac{\langle (\Delta \hat{n})^2 \rangle - \langle \hat{n} \rangle}{\langle \hat{n} \rangle}, \quad (19)$$

where $\hat{n} = \hat{a}^\dagger \hat{a} = (\hat{q}^2 + \hat{p}^2)/2 - 1/2$, and $\langle (\Delta \hat{n})^2 \rangle \equiv \langle \hat{n}^2 \rangle - \langle \hat{n} \rangle^2$. For $Q = 0$, photons are in a coherent state and obey trivial Poisson statistics, while for $Q > 0$, they obey super-Poissonian statistics, which have a classical

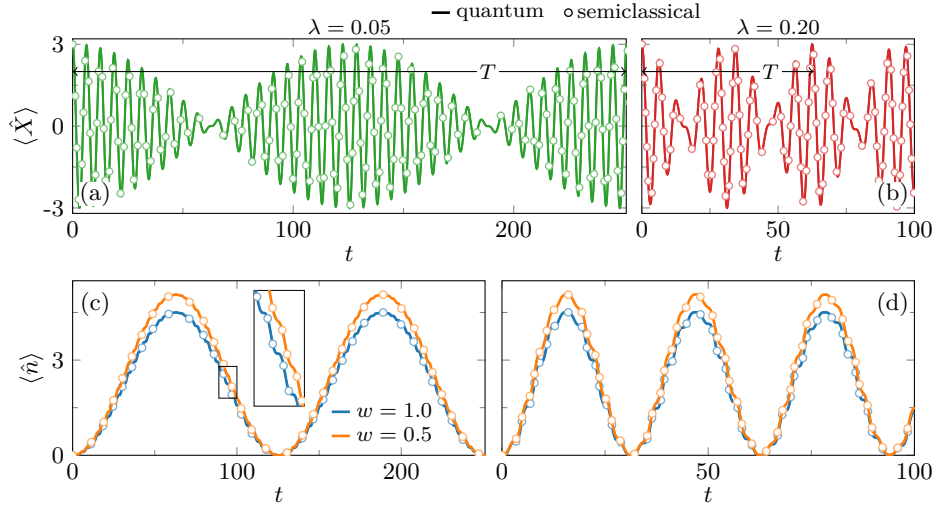


FIG. 3. (a,b) Expectation values of the matter CM quadrature at resonance, $\langle \hat{X}(t) \rangle$ [see Eq. (20), $\gamma = 1$, $X_0 = 3$, $w = 0.5$] for two light-matter coupling regimes, strong and ultrastrong. $\langle \hat{X}(t) \rangle$ is independent of w . The beating period is defined as $T \equiv 2\pi/(\bar{\Delta}/2)$. At resonance, $\bar{\Delta} = \lambda$, and $T = 4\pi/\lambda \approx 251, 63$ for (a) and (b), respectively, illustrating the strong dependence on the collective coupling, λ . (c,d) The generated photon number expectation values at resonance for squeezed and non-squeezed matter. The inset in (c) shows the presence of high-frequency oscillations. The quantum and semiclassical results agree in all cases.

analogue. When $Q < 0$, the photons follow sub-Poissonian statistics, a hallmark of quantum light with no classical counterpart [83, 98, 99]. Under certain conditions—specifically, in a single-mode cavity when the field is in a stationary state, the Mandel Q function is related to the zero-time-delay second-order correlation function $g^{(2)}(0)$ by $Q = \langle \hat{n} \rangle [g^{(2)}(0) - 1]$ [83, 100]. The quantity $g^{(2)}(0)$ is frequently used to infer photon correlations and quantifies the likelihood of simultaneous photon detection events. Here, however, we focus exclusively on the Mandel Q parameter as a measure of the spread of the photon number distribution and do not attempt to relate it to $g^{(2)}(0)$.

Note that quadrature squeezing without displacement in the phase space does not result in sub-Poissonian statistics [83]. Geometrically, $\langle (\Delta \hat{n})^2 \rangle \leq \langle \hat{n} \rangle$ occurs when the radial variance of the phase space distribution is lower than the average radial displacement. In Fig. 2, the *matter* is initially squeezed with $Q_{\text{mat}} < 0$. Note that Q_{mat} is also defined by Eq. (19), but with $\hat{n} = \hat{b}^\dagger \hat{b} = (\hat{X}^2 + \hat{P}^2)/2 - 1/2$ being the number operator for the matter CM states. While matter and light states exchange, the nonclassical features emerge in the light degree of freedom, manifesting in $Q < 0$. The effective transfer of the matter state, characterized by a negative Q parameter, into the cavity mode, is one of the key findings of this work.

A. Beating and light-matter resonance

Next, we explore the dynamics of the subsystems in more detail. Fig. 3(a,b) shows the expectation value of the matter CM position quadrature, $\langle \hat{X}(t) \rangle$, at resonance with the cavity ($\gamma = 1$), in strong (ultrastrong) light-matter coupling regime, $\lambda = 0.05$ ($\lambda = 0.2$). According to the Ehrenfest theorem [96, 97], $\langle \hat{X}(t) \rangle$ equals the classical solution $X(t)$ of a single particle with initial position X_0 , and zero momentum (App. C)

$$\frac{\langle \hat{X}(t) \rangle}{X_0} = \cos \left[\frac{\bar{\Sigma} t}{2} \right] \cos \left[\frac{\bar{\Delta} t}{2} \right] + \beta \sin \left[\frac{\bar{\Sigma} t}{2} \right] \sin \left[\frac{\bar{\Delta} t}{2} \right], \quad (20)$$

where $\bar{\Sigma} \equiv \Omega_+ + \Omega_-$, $\bar{\Delta} \equiv \Omega_+ - \Omega_-$ is the vacuum Rabi splitting (VRS), $\bar{\Delta} \leq \bar{\Sigma}$, and $\beta = (\Omega_+^2 + \Omega_-^2 - 2)/(\bar{\Sigma} \bar{\Delta})$. The higher frequency, $\bar{\Sigma}$, defines the rotation period of the phase space distributions in Fig. 2. The VRS, on the other hand, defines the long beating period $T = 2\pi/(\bar{\Delta}/2)$ during which $\langle \hat{X} \rangle$ exhibits slow beatings, and state transfer occurs. This emergent long timescale, proportional to the VRS, depends on the collective coupling and, consequently, the number of particles, $\lambda \propto \sqrt{N}$ (at resonance, $\bar{\Delta} = \lambda$).

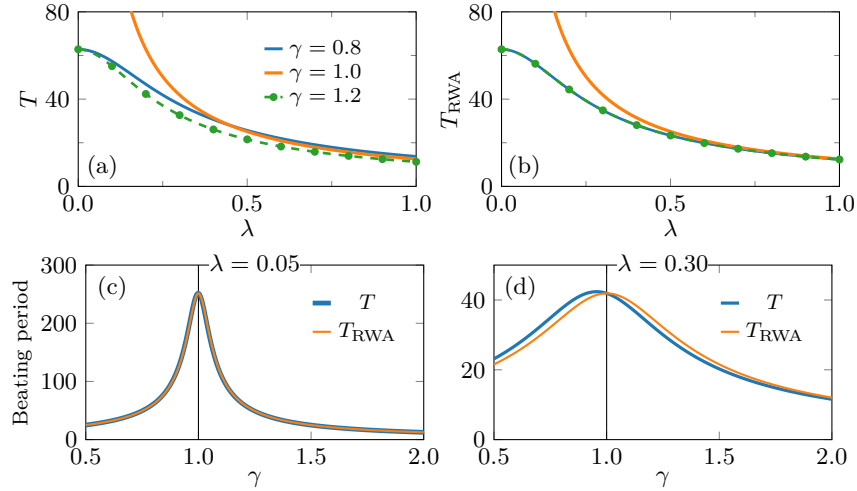


FIG. 4. Dependence of the beating periods, $T \equiv 4\pi/(\Omega_+ - \Omega_-)$ [Eq. (17)] and $T_{\text{RWA}} \equiv 4\pi/(\Omega_{\text{RWA},+} - \Omega_{\text{RWA},-})$ [Eq. (B2)] on (a,b) λ and (c,d) γ . T has a distinctive asymmetry as the cavity frequency is scanned through resonance. In contrast, T_{RWA} is independent of the sign of the detuning, such that the $\gamma = 0.8, 1.2$ curves in (b) overlap, and the RWA curve in (d) is symmetric about the point $\gamma = 1$.

In addition to the collective nature of the beating phenomenon, it is important to highlight the dependence of T on the detuning. In Fig. 4(c), we observe that when light and matter excitations are in resonance ($\gamma = 1$), the beating period reaches its maximum, and the respective beating frequency is suppressed. This shows that the collective dynamics of an ensemble of particles resonantly coupled to a cavity can be significantly modified even in vacuum, i.e., without an external driving field. Similar modifications of dynamics at resonance have been observed in chemical reactions of collectively coupled molecules under VSC [21, 22, 30, 32–34]. As described in Section II, the HH also applies to harmonic molecules strongly coupled to a cavity mode. Thus, our work could hint at the observed resonant modification of reactions in polaritonic chemistry [30, 77, 78]. Notably, the beating period exhibits a sharp resonance in the strong coupling regime ($\lambda = 0.05$), while in the ultrastrong regime ($\lambda = 0.2$), the peak broadens as shown in Fig. 4(d). This is due to CRT, on which we focus next.

B. Effects of the Counter-rotating Terms on Dynamical Observables

The CRT make the polariton avoided crossing sensitive to the sign of the relative detuning, $\gamma - 1 = (\omega - \Omega)/\Omega$, and the difference between red- and blue-shifted cavity cases increases with λ (App. B). This is a characteristic of the ultrastrong coupling regime [3, 85]. Consequently, the beating period, T , is also sensitive to the detuning sign, as shown in Fig. 4(a). In contrast, under the rotating wave approximation (RWA), when the terms proportional to $\lambda\hat{a}^\dagger\hat{b}^\dagger$, $\lambda\hat{a}\hat{b}$ and λ^2 are omitted from Eq. (15)], $\bar{\Delta}$ is independent of the detuning sign. Fig. 4(b) shows T_{RWA} , which remains the same for detunings of either sign.

Fig. 4(c) demonstrates that the RWA is a good approximation for $\lambda < 0.1$, as $T \approx T_{\text{RWA}}$, which is expected. However, the asymmetry of T around $\gamma = 1$ becomes evident in panel (d). Additionally, the prefactor β in Eq. (20) vanishes at resonance under the RWA (App. C). The asymmetries in the time-dependent matter CM quadrature are dynamic manifestations of the polariton branch asymmetry around $\gamma = 1$. Although the asymmetries of $\langle \hat{X}(t) \rangle$ arise from ultrastrong coupling, they are not inherently quantum effects. As mentioned earlier, in a system of coupled harmonic oscillators, the normal-mode frequencies, Ω_\pm , and the first moments are determined by the classical solution, meaning similar features can be observed even in a pair of coupled classical oscillators. Therefore, next, we consider time-dependent observables defined in terms of the second moments of the light probability distribution to identify potential quantum effects.

Fig. 3(c,d) shows the evolution of the photon number expectation value, $\langle \hat{n}(t) \rangle$ at resonance ($\gamma = 1$). The local maxima correlate to when the phase space distribution is farthest from the origin. The time-averaged

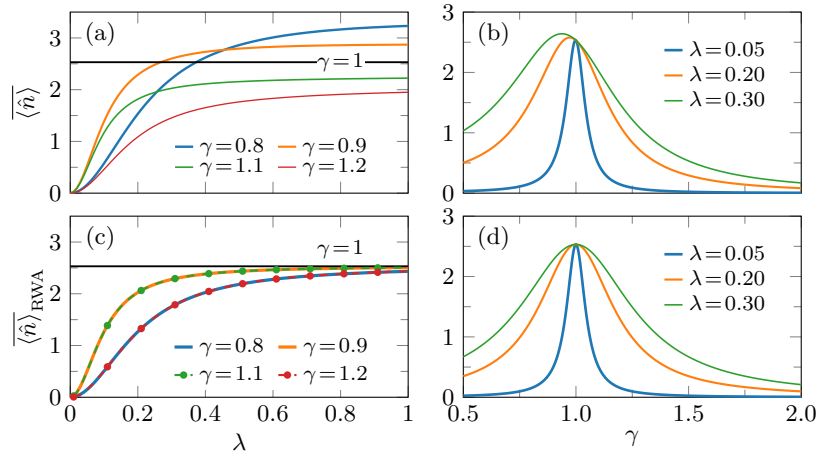


FIG. 5. (a,b) Dependence of average photon number in Eq. (21) on λ and γ . (c,d) The same as in (a,b), but under RWA. At resonance, the average number of photons becomes independent of the coupling strength, λ in both the full system and under RWA—all graphs in panels (b) and (d) overlap at $\gamma = 1$. Note that in panel (d), the functions are symmetric Lorentzians centered at $\gamma = 1$.

expectation value is given by (for the full expression, see App. E)

$$\overline{\langle \hat{n} \rangle} \approx \Delta \overline{\langle \hat{n} \rangle} = \lambda^2 f_1(w^{-2} - 1) + \lambda^2 f_2(2X_0^2 + w^2 - 1), \quad (21)$$

where $\Delta \langle \hat{n}(t) \rangle \equiv \langle \hat{n}(t) \rangle - \langle \hat{n}(t; X_0 = 0, w = 1) \rangle$. To simplify the expression, we subtract the relatively small contribution from the average photon number when the CM is in the ground state. Here, $f_{1,2}$ are functions of Ω_{\pm} . At resonance, $\Delta \overline{\langle \hat{n} \rangle}(\gamma = 1) = X_0^2/4 + (w - w^{-1})^2/8$. For negligible matter squeezing ($w \approx 1$), $\Delta \overline{\langle \hat{n} \rangle} \approx (2\lambda^2 f_2)X_0^2$, and the average number of generated photons is determined by the initial CM shift, X_0 . Fig. 5(a,b) shows the dependence of $\Delta \overline{\langle \hat{n} \rangle}$ on λ and γ . The average photon number is asymmetric relative to the resonance point and fewer photons are generated, on average, for $\gamma > 1$. This asymmetry has important implications for the photon number distribution as well because, as we discuss next, the Q function is more negative in the blue-shifted cavity.

Under RWA, $\overline{\langle \hat{n} \rangle}_{\text{RWA}} = \lambda^2 f_{\text{RWA}}[2X_0^2 + (w - w^{-1})^2]$, and $f_{\text{RWA}} = 1/[8(\gamma - 1)^2 + 8\lambda^2]$ is symmetric about $\gamma = 1$ (App. E). Fig 5(c,d) shows the dependencies of $\overline{\langle \hat{n} \rangle}_{\text{RWA}}$. In panel (c), the $\gamma = 0.8, 1.2$ and $\gamma = 0.9, 1.1$ curves overlap, while panel (d) demonstrates the symmetric Lorentzian function. The blue curves ($\lambda = 0.05$) in panels (b) and (d) are practically indistinguishable, suggesting that the RWA is a good approximation in the weak coupling regime ($\lambda \ll 1$).

The asymmetries in the time-averaged photon number reflect the effects of ultrastrong light-matter coupling. In contrast to the first moments, the photon number explicitly depends on the quantum uncertainty in position- and momentum-related quadratures. The average photon number is an experimentally accessible observable (for details, see Sec. V) and thus allows probing effects beyond RWA in quantum systems.

C. Mandel Q Function

Next, we focus on the Mandel Q function, which quantifies nonclassicality, indicated by negative values of Q . Fig. 6(a,b) illustrates the evolution of the photon Q function at resonance, when Q attains negative values only when CM is both shifted *and* quadrature-squeezed in X (i.e., when $w < 1$). Qualitatively, Fig. 2 suggests that the minimum of Q is connected to the initial value of Q_{mat} , given by $Q_{\text{mat}}(0) = (w^2 - 1)[1 + \mathcal{O}(X_0^{-2})]$ (App. F). While $\overline{\langle \hat{n} \rangle}$ in Eq. (21) scales with X_0^2 , the initial Q_{mat} approaches a constant as X_0 increases, leading to the saturation of the minimal attainable Q values.

The time-averaged photon Mandel function, $\overline{Q} \equiv \lim_{\tau \rightarrow \infty} \tau^{-1} \int_0^\tau Q(t) dt$, is shown in Fig. 6(c-e) for a range of X_0 and w values. \overline{Q} is negative on either side of the resonance for an initially shifted and quadrature-squeezed matter state. Notably, Q may attain negative values for an initially quadrature-squeezed matter

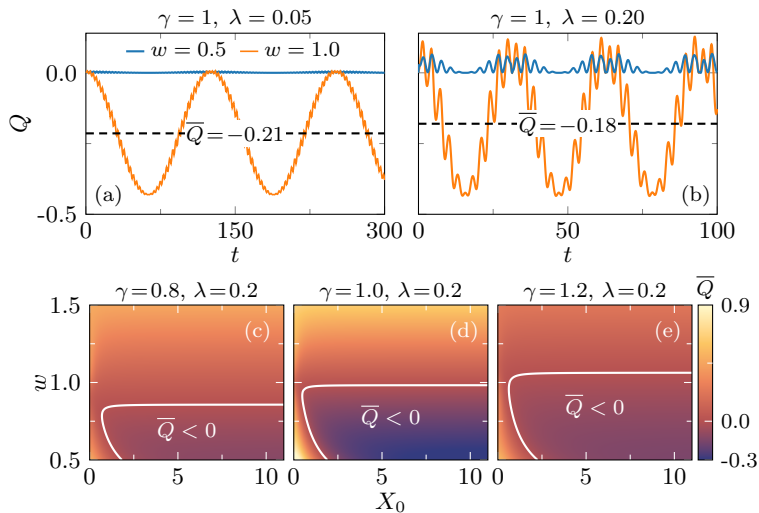


FIG. 6. (a,b) Mandel Q functions for the same w and λ values. Importantly, for $w = 0.5$, the time-averaged Q function, \bar{Q} attains negative values. (c-e) The dependence of photon \bar{Q} on the initial displacement and width of the matter CM state is shown before (c), at (d), and after (e) the cavity resonance for strong cavity coupling. The nonclassical features of the photon state primarily occur for $w < 1$. At resonance in (d), the state transfer is most efficient. The asymmetry between (c) and (e) vanishes in the RWA (see App. F), and $\bar{Q} < 0$ can be achieved only for $w < 1$.

state even without the diamagnetic term ($\propto \lambda^2$) and under the RWA. However, under the RWA, the asymmetry between (c) and (e) disappears, and negative \bar{Q} can be achieved only for $w < 1$ (App. F).

IV. SCHEME II. GENERATION OF NONCLASSICALITY FROM A COHERENT CAVITY

An alternative approach for generating nonclassical states involves initializing the system with the matter CM in its ground state and the cavity in a coherent state, $|\alpha\rangle$. Fig. 7 illustrates the evolution of the phase space distributions of matter CM (top row) and light (bottom row) in Scheme II. Initially, both Q and Q_{mat} are zero, as the system begins in a trivial state without any correlations. In this scenario, the counter-rotating interaction terms are crucial in generating sub-Poissonian distributions in the motional states of matter or photon number states (App. F).

Over time, the matter and light distributions periodically elongate (squeeze); however, during maximal elongation, the matter phase space distribution aligns approximately along the line connecting its center to the origin, while the light distribution is oriented perpendicularly. As previously noted, the Q function becomes negative when the radial variance of the phase space distribution is less than the radial displacement. In this scenario, only the photon Q function attains negative values. In contrast to the resonance case shown in Fig. 2, the state transfer is only partial due to the large detuning. The matter phase space distribution doesn't reach the initial radial displacement of the light distribution, and the light distribution does not collapse to the origin.

Fig. 8 shows the time averaged photon \bar{Q} (top panels) and matter \bar{Q}_{mat} (bottom panels). \bar{Q} is sensitive to the phase of α , negative \bar{Q} is obtained before (after) the resonance for coherent states with sufficiently large $\text{Re}[\alpha]$ ($\text{Im}[\alpha]$). The Q functions reach saturation along the real or imaginary axes. At resonance, both \bar{Q} and \bar{Q}_{mat} remain non-negative. Additionally, a clear asymmetry appears between the red and blue detuned cavities in panels (a) and (c). This asymmetry increases with λ , and, in the case of photons, culminates with the complete absence of $\bar{Q} < 0$ in the red-shifted cavity in the ultra-strong coupling regime ($\lambda = 0.5$, see App. F).

Remarkably, under initial conditions where the photon $\bar{Q} \geq 0$ in Fig. 8(a,c), \bar{Q}_{mat} attains negative values. In other words, even when the sub-Poissonian PND is not achieved, the coherent state is partially transferred to the matter subsystem, simultaneously developing the sub-Poissonian distribution of motional states of the *matter* CM. The generation of nonclassical states in light and matter, starting from a coherent state of light,

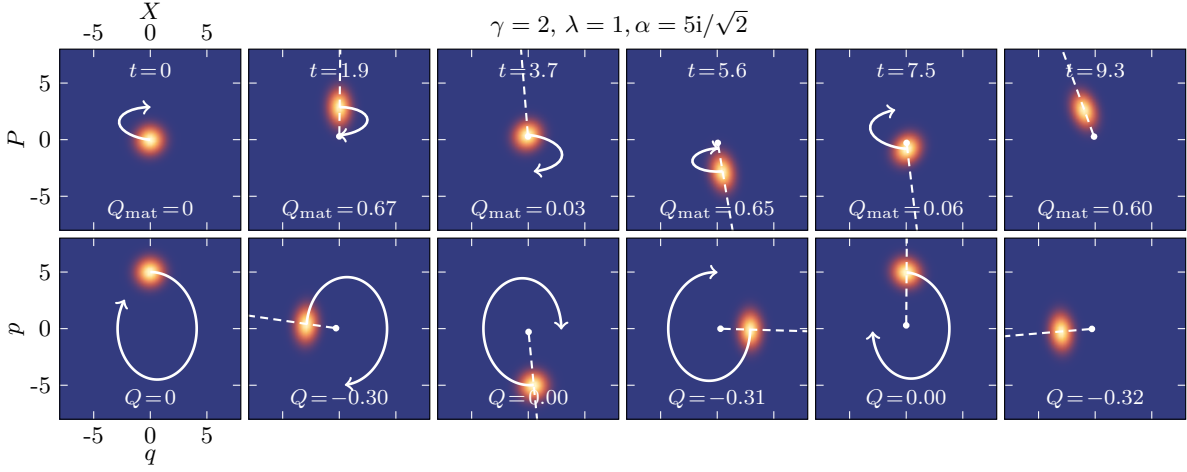


FIG. 7. Snapshots of evolving phase space distribution of matter (X, P , upper row) and cavity field (q, p , bottom row). The initial state in Scheme II is a product of matter CM ground state and cavity coherent state, $|\alpha\rangle$. The arrows show the trajectories of the distribution centers. The dashed lines pass through the origin and distribution centers in each panel. Note that the matter distributions approximately align with the dashed lines, while the light distributions are perpendicular. The values of detuning and coupling constant are exaggerated to highlight the effect.

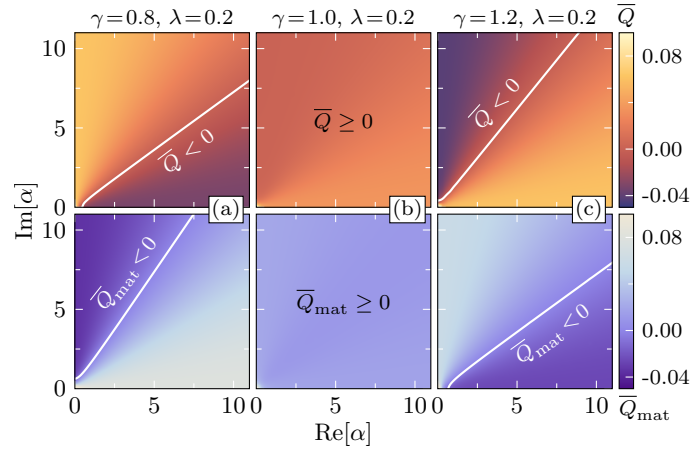


FIG. 8. The dependence of photon \bar{Q} (top panels) and the matter \bar{Q}_{mat} (bottom panels) on the initial coherent state, $|\alpha\rangle$. Sub-Poissonian distributions of photon and motional states are achieved off-resonance in (a) and (c). With increasing $\text{Re}[\alpha]$ and $\text{Im}[\alpha]$ components, the sub-Poissonian distributions saturate. At resonance, both photon and matter Mandel parameters are positive.

represents a key finding of this work.

The average number of photons, $\langle \hat{n} \rangle$, is also sensitive to the phase of α and shows trends similar to those of \bar{Q} . The symmetries of $\langle \hat{n} \rangle$ can be accessed via $\delta \langle \hat{n} \rangle \equiv \langle \hat{n}(\alpha = C) \rangle - \langle \hat{n}(\alpha = iC) \rangle$, where $C > 0$. $\delta \langle \hat{n} \rangle$ measures the difference in average photon number between the initial coherent state with $\text{Re}[\alpha]$ vs. $\text{Im}[\alpha]$, and it is given by

$$\delta \langle \hat{n} \rangle = \lambda^2 C^2 \frac{(2\gamma + \lambda^2)(\Omega_+^2 + \Omega_-^2) - 4\gamma}{4\bar{\Sigma}^2 \bar{\Delta}^2}. \quad (22)$$

Fig. 9 shows the dependence of $\delta \langle \hat{n} \rangle / C^2$ on the system parameters. Here, the value of C is large enough to saturate the Q parameter. On average, the cavity is populated with fewer photons for $\text{Re}[\alpha]$ ($\text{Im}[\alpha]$), before (after) the resonance.

Moreover, the asymmetry of $|\delta \langle \hat{n} \rangle|$ increases with λ . In the rotating wave approximation, $\delta \langle \hat{n} \rangle = 0$. To our knowledge, this asymmetry in photon generation as light-matter coupling enters the ultrastrong regime has

not been previously discussed. This phenomenon could potentially be tested in Landau polariton systems, where ultrastrong coupling has been demonstrated [3, 8, 12, 85]. Such observation would provide clear evidence of the dynamical manifestation of ultrastrong coupling, extending our understanding of this regime beyond conventional spectroscopic methods.

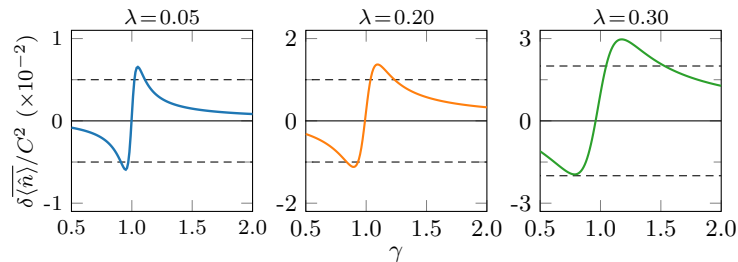


FIG. 9. Dependence of $\delta\langle\hat{n}\rangle/C^2$ in Eq. (22) on γ . In all cases, on average, the cavity is populated with more photons starting from a coherent state with imaginary (real) α below (above) resonance. The asymmetry of $|\delta\langle\hat{n}\rangle|$ about $\gamma = 1$ increases with λ .

V. HOW TO ACCESS THE NONCLASSICAL STATES

In Scheme I, the nonclassical photons generated in the cavity can be extracted by making one of the cavity mirrors semi-transparent [86, 101]. The output field is obtained by employing the input-output formalism, which assumes a bilinear coupling to the bath degrees of freedom (cavity environment) through the field operators \hat{a} and \hat{a}^\dagger , with a constant coupling proportional to $\sqrt{\kappa}$. In this framework, the relationship between the cavity field operator $\hat{a}(t)$ and the output field operator, $\hat{d}_{\text{out}}(t)$ is given by [102]

$$\dot{\hat{a}} = -i[\hat{a}, \hat{\mathcal{H}}] + \frac{\kappa}{2}\hat{a} - \sqrt{\kappa}\hat{d}_{\text{out}}. \quad (23)$$

The bath can also feed energy into the cavity through the operator $\hat{d}_{\text{in}}(t)$. The input-output relation states that $\hat{d}_{\text{out}}(t) - \hat{d}_{\text{in}}(t) = \sqrt{\kappa}\hat{a}(t)$. In practice, the effect of coupling on the system can be formulated in terms of the master equation for the reduced density matrix of the system, $\hat{\rho}$. In the low-temperature limit ($k_B T \ll \hbar\omega_i$, where ω_i is an eigenfrequency of the system) and weak system-bath coupling, the master equation becomes [102]

$$\dot{\hat{\rho}} = -i[\hat{\mathcal{H}}, \hat{\rho}] + \frac{\kappa}{2}(2\hat{a}\hat{\rho}\hat{a}^\dagger - \hat{a}^\dagger\hat{a}\hat{\rho} - \hat{\rho}\hat{a}^\dagger\hat{a}). \quad (24)$$

Eq. (24) can be used to write the master equation for the annihilation operator, \hat{a} , $\dot{\hat{a}} = -i[\hat{a}, \hat{\mathcal{H}}] - (\kappa/2)\hat{a}$. Substituting this into Eq. (23) yields $\hat{d}_{\text{out}} = \sqrt{\kappa}\hat{a}$. Therefore, the number of photons leaking from the cavity is proportional to the number inside, $\langle\hat{n}_{\text{out}}(t)\rangle = \kappa\langle\hat{n}(t)\rangle$. Similarly, $Q_{\text{out}}(t) = \kappa Q(t)$.

Fig. 10 shows expectation values obtained by numerically solving Eq. (24). The observables exhibit persistent oscillations, exponentially decaying at an approximate rate of $\kappa/2$ (assuming $\kappa \ll \Omega$). The time-averaged expectation value of the photons outside the cavity can be approximated as $\overline{\langle\hat{n}_{\text{out}}(t)\rangle} \approx \kappa\overline{\langle\hat{n}\rangle} \exp(-\kappa t/2)$ where $\overline{\langle\hat{n}\rangle}$ is given by Eq. (21). Constrained optimization can be employed to simultaneously minimize Q_{out} and maximize $\langle\hat{n}_{\text{out}}\rangle$, thereby optimizing detection efficiency, but this is beyond the scope of the present study.

Alternatively, in Scheme II, the sub-Poissonian distribution of the matter CM states can be directly observed via spectroscopic methods, such as sideband spectroscopy for trapped atomic ions [62, 65]. Light and matter can be decoupled by introducing a large detuning to measure the properties of matter independently. The method and the details for introducing detuning will depend on the system and experimental setup.

VI. CONCLUSIONS AND OUTLOOK

By leveraging the formation of polaritons in strongly and ultrastrongly coupled light-matter systems, we propose two initialization schemes to generate and effectively exchange nonclassical states of matter and light.

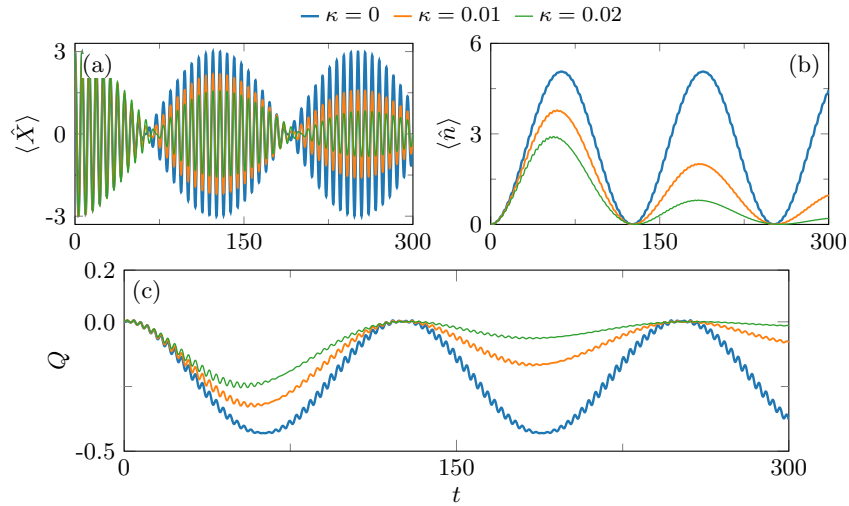


FIG. 10. Expectation values of (a) matter CM X quadrature, (b) photon number, and (c) photon Mandel Q in the presence of cavity loss. The results were obtained by numerically solving Eq. (24). Parameters: $\gamma = 1$, $X_0 = 3$, $w = 0.5$.

In the first scheme, an initially displaced and quadrature-squeezed matter CM state is dynamically transferred to the cavity mode, producing nonclassical photons that can be extracted by making one of the cavity mirrors semi-transparent. This scheme builds upon the ability to create coherent and quadrature-squeezed matter states in ion traps (e.g., see [62]).

The second initialization scheme relies on the ultrastrong coupling effects (i.e., on the presence of CRT in the Hamiltonian), which generate sub-Poissonian distributions of photon or matter states, starting from a coherent cavity state. This shows that an ultrastrongly coupled light-matter system acts as a generator that transforms a coherent photonic state, devoid of nonclassical characteristics, into a nonclassical state of light or matter. This demonstrates a clear quantum advantage of the ultrastrong coupling regime [3, 85] and suggests novel pathways for hybrid, polaritonic quantum technologies. For example, one could envision protocols where matter is prepared in such a state that the system evolves into a macroscopic cat state [91] or a photonic cluster state [92], which can be used for quantum information and computation.

On the matter side, the population distribution of the matter states can be measured spectroscopically after decoupling the matter from the cavity. Additional manifestations of the ultrastrong coupling effects are the distinctive asymmetries in dynamical observables, such as average photon number and Mandel Q parameter, emerging as the cavity frequency is scanned through the resonance. These CRT-induced asymmetries provide a novel, dynamical perspective on the ultrastrong coupling regime typically probed by transmission spectroscopy. To our knowledge, such dynamic asymmetries have not been reported elsewhere.

The considered schemes can act as probes of quantum dynamics under strong or ultrastrong light-matter coupling in microscopic and mesoscopic systems. The coupling to light in such systems differs from that in typical optomechanical systems [48]. Initializing the cavity field in non-trivial states may enable new quantum control schemes for chemical processes in molecular systems under VSC. This could lead to applications in catalysis or the development of novel reaction pathways influenced by quantum states of light. Similarly, for Landau levels coupled to the cavity mode, strong light-matter interactions can transfer states of light to the electronic subsystem's collective (CM) mode, offering new ways to control electronic properties. Once a strong-ultrastrong coupling regime between the trapped ion's motion and the cavity mode is achieved, nonclassical photons could be potentially generated from squeezed motional states of ions. Nonclassical photonic states are important for sensing beyond the standard quantum limit [87–90].

We anticipate that our analysis will inspire further experimental and theoretical investigations of the dynamics in various strongly and ultrastrongly coupled light-matter systems, ultimately advancing the field of quantum science and technology and bridging it with polaritonic chemistry [22, 77, 78] and cavity quantum materials [16, 30].

ACKNOWLEDGMENTS

I.T., V.R., and H.R.S. acknowledge support from the NSF through a grant for ITAMP at Harvard University. I.T. was also supported by an NSF subcontract No. 3357 at the Smithsonian Astrophysical Observatory. J.C. acknowledges support from the NSF (Grants No. CHE1800301 and No. CHE2324300), and the MIT Sloan Fund.

Appendix A: Mapping to the Hopfield Hamiltonian for Different Systems

In this Appendix, we detail the intermediate steps involved in transforming the Hamiltonians of the various systems in Section II into the HH.

1. Cold Trapped Ions

The collective coupling between the trapped ions and the cavity field emerges by transforming the Hamiltonian in Eq. (1) to the CM frame. A similar transformation will also be used for the other systems considered later; so, we will show all the steps here. For mathematical convenience, we utilize a symmetric definition with respect to \sqrt{N} for the coordinates in the CM frame [94]

$$\hat{\mathbf{R}} = \frac{1}{\sqrt{N}} \sum_{i=1}^N \hat{\mathbf{r}}_i \quad \text{and} \quad \hat{\mathbf{r}}_j = \frac{\hat{\mathbf{r}}_1 - \hat{\mathbf{r}}_j}{\sqrt{N}} \quad \text{with} \quad j > 1. \quad (\text{A1})$$

The momenta of the particles in the new coordinate system are $\nabla_1 = (\nabla_{\mathbf{R}} + \sum_{j=2}^N \tilde{\nabla}_j)/\sqrt{N}$ and $\nabla_j = (\nabla_{\mathbf{R}} - \tilde{\nabla}_j)/\sqrt{N}$ with $j > 1$. The kinetic energy terms in the new frame are given by

$$\sum_{i=1}^N \nabla_i^2 = \nabla_{\mathbf{R}}^2 + \frac{1}{N} \sum_{j=2}^N \tilde{\nabla}_j^2 + \frac{1}{N} \sum_{j,k=2}^N \tilde{\nabla}_j \cdot \tilde{\nabla}_k. \quad (\text{A2})$$

In the new coordinates, the cavity field couples only to the CM momentum, $\hat{\mathbf{A}} \cdot \sum_{i=1}^N \nabla_i = \sqrt{N} \hat{\mathbf{A}} \cdot \nabla_{\mathbf{R}}$, while the scalar trapping potential separates into two parts, one depending on the CM coordinate and the other one on the relative coordinates, without cross-terms between the two

$$\sum_{i=1}^N \hat{\mathbf{r}}_i^2 = \hat{\mathbf{R}}^2 + N \sum_{j=2}^N \hat{\mathbf{R}}_j^2 - \left[\sum_{j=2}^N \hat{\mathbf{R}}_j \right]^2. \quad (\text{A3})$$

The two-body interaction $W(\hat{\mathbf{r}}_i - \hat{\mathbf{r}}_l)$ depends only on the relative distances and thereby does not affect the cavity-induced CM motion. In the CM frame, it is given by

$$\sum_{i<l}^N W(\hat{\mathbf{r}}_i - \hat{\mathbf{r}}_l) = \sum_{1<l}^N W(\sqrt{N} \hat{\mathbf{r}}_l) + \sum_{2 \leq i < l}^N W\left(\sqrt{N}(\hat{\mathbf{r}}_i - \hat{\mathbf{r}}_l)\right). \quad (\text{A4})$$

The analysis above shows that the Hamiltonian separates into two parts, $\hat{H}_{\text{ion}} = \hat{H}_{\text{ion-cm}} + \hat{H}_{\text{ion-rel}}$, where (i) $\hat{H}_{\text{ion-cm}}$, describes the CM coupling to the quantized field $\hat{\mathbf{A}}$, and (ii) $\hat{H}_{\text{ion-rel}}$, describes the dynamics of the relative coordinates, decoupled from $\hat{\mathbf{A}}$ and the CM. The two parts are given by

$$\begin{aligned} \hat{H}_{\text{ion-cm}} &= \frac{1}{2m} (i\hbar \nabla_{\mathbf{R}} + g_0 \sqrt{N} \hat{\mathbf{A}})^2 + \frac{m\Omega^2}{2} \hat{\mathbf{R}}^2 + \sum_{\nu=x,y} \hbar\omega \left(\hat{a}_\nu^\dagger \hat{a}_\nu + \frac{1}{2} \right), \\ \hat{H}_{\text{ion-rel}} &= -\frac{\hbar^2}{2mN} \sum_{j=2}^N \tilde{\nabla}_j^2 - \frac{\hbar^2}{2mN} \sum_{j,k=2}^N \tilde{\nabla}_j \cdot \tilde{\nabla}_k + \frac{mN\Omega^2}{2} \sum_{j=2}^N \hat{\mathbf{r}}_j^2 \\ &\quad - \frac{m\Omega^2}{2} \left[\sum_{j=2}^N \hat{\mathbf{r}}_j \right]^2 + \sum_{1<l}^N W(\sqrt{N} \hat{\mathbf{r}}_l) + \sum_{2 \leq i < l}^N W\left(\sqrt{N}(\hat{\mathbf{r}}_i - \hat{\mathbf{r}}_l)\right). \end{aligned} \quad (\text{A5})$$

In addition, it is crucial to demonstrate that the CM and relative distance degrees of freedom are independent by checking the commutation relations between their coordinates and momenta. Using the chain rule, we find the derivatives in the CM frame

$$\nabla_{\mathbf{R}} = \frac{1}{\sqrt{N}} \sum_{i=1}^N \nabla_i \quad \text{and} \quad \tilde{\nabla}_j = \frac{1}{\sqrt{N}} \sum_{i=1}^N \nabla_i - \sqrt{N} \nabla_j \quad \text{with } j > 1, \quad (\text{A6})$$

It is clear that the momenta in the new frame of reference commute, $[\nabla_{\mathbf{R}}, \tilde{\nabla}_j] = 0$. It can also be shown that the momenta and coordinates are independent since $[\nabla_{\mathbf{R}}, \hat{\mathbf{r}}_j] = 0$ and $[\tilde{\nabla}_j, \hat{\mathbf{R}}] = 0$. Thus, we focus on the CM part to describe the cavity-matter dynamics. Since the polarization vectors of the photon field lie in the (x, y) plane, the z direction of the system becomes trivial. The light-matter Hamiltonian then describes a system of interacting harmonic oscillators, and importantly, the x and y directions are independent,

$$\hat{H}_{\text{ion-cm}} = \sum_{\nu=x,y} \left[-\frac{\hbar^2}{2m} \partial_{R_\nu}^2 + \frac{ig_0\hbar}{m} \sqrt{N} \hat{A}_\nu \partial_{R_\nu} + \frac{m\Omega^2}{2} \hat{R}_\nu^2 + \frac{Ng_0^2}{2m} \hat{A}_\nu^2 + \hbar\omega \left(\hat{a}_\nu^\dagger \hat{a}_\nu + \frac{1}{2} \right) \right]. \quad (\text{A7})$$

To avoid any confusion, note that $\hat{\mathbf{R}} = (\hat{R}_x, \hat{R}_y) = (\hat{X}, \hat{Y})$, $\nabla_{\mathbf{R}} = (\partial_{R_x}, \partial_{R_y}) = (\partial_X, \partial_Y)$ and $\hat{\mathbf{A}} = (\hat{A}_x, \hat{A}_y)$. Consequently, we can treat only one of the system's equivalent directions. Thus, the Hamiltonian that captures the ion-cavity dynamics is given by

$$\hat{H}_{\text{ion-cm}} = -\frac{\hbar^2}{2m} \partial_X^2 + \frac{m\Omega^2}{2} \hat{X}^2 + \frac{ig_0\hbar}{m} \sqrt{N} \hat{A}_x \partial_X + \frac{Ng_0^2}{2m} \hat{A}_x^2 + \hbar\omega \left(\hat{a}_x^\dagger \hat{a}_x + \frac{1}{2} \right). \quad (\text{A8})$$

Finally, in terms of the matter annihilation operators

$$\hat{b}_x = \sqrt{\frac{m\Omega}{2\hbar}} \left(\hat{X} + \frac{\hbar}{m\Omega} \partial_X \right), \quad (\text{A9})$$

the CM Hamiltonian attains the form of the well-known HH [54, 85]

$$\hat{H}_{\text{ion-cm}} = \hbar\Omega \left(\hat{b}_x^\dagger \hat{b}_x + \frac{1}{2} \right) - i\sqrt{\frac{\hbar\Omega g_0^2 N}{2m}} \hat{A}_x (\hat{b}_x^\dagger - \hat{b}_x) + \frac{Ng_0^2}{2m} \hat{A}_x^2 + \hbar\omega \left(\hat{a}_x^\dagger \hat{a}_x + \frac{1}{2} \right). \quad (\text{A10})$$

2. Landau Levels

Next, we provide the details about the light-matter dynamics of 2degs coupled to the cavity field defined in Eq.(6). The interaction term between the cavity field and the dynamical momentum of electrons is given by

$$\hat{\mathbf{A}} \cdot \sum_{i=1}^N i\hbar \nabla_i + e\hat{\mathbf{A}}_{\text{ext}}(\hat{\mathbf{r}}_i) = \sqrt{N} \hat{\mathbf{A}} \cdot [i\hbar \nabla_{\mathbf{R}} + e\hat{\mathbf{A}}_{\text{ext}}(\hat{\mathbf{R}})]. \quad (\text{A11})$$

In terms of new coordinates, the sum of squares of the external field is given by

$$\sum_{i=1}^N \hat{\mathbf{A}}_{\text{ext}}^2(\hat{\mathbf{r}}_i) = \hat{\mathbf{A}}_{\text{ext}}^2(\hat{\mathbf{R}}) + N \sum_{j=2}^N \hat{\mathbf{A}}_{\text{ext}}^2(\hat{\mathbf{r}}_j) - \left[\sum_{j=2}^N \hat{\mathbf{A}}_{\text{ext}}(\hat{\mathbf{r}}_j) \right]^2. \quad (\text{A12})$$

The bilinear term between the magnetic field and the momenta is given by

$$\sum_{i=1}^N \hat{\mathbf{A}}_{\text{ext}}(\hat{\mathbf{r}}_i) \cdot \nabla_i = \hat{\mathbf{A}}_{\text{ext}}(\hat{\mathbf{R}}) \cdot \nabla_{\mathbf{R}} + \sum_{j=2}^N \hat{\mathbf{A}}_{\text{ext}}(\hat{\mathbf{r}}_j) \cdot \tilde{\nabla}_j. \quad (\text{A13})$$

Collecting the terms, we find that the Hamiltonian in the new frame is a sum of two terms, $\hat{H}_{2\text{deg}} = \hat{H}_{2\text{deg-cm}} + \hat{H}_{2\text{deg-rel}}$, where: (i) the center of mass term, $\hat{H}_{2\text{deg-cm}}$ includes the coupling to the quantized field

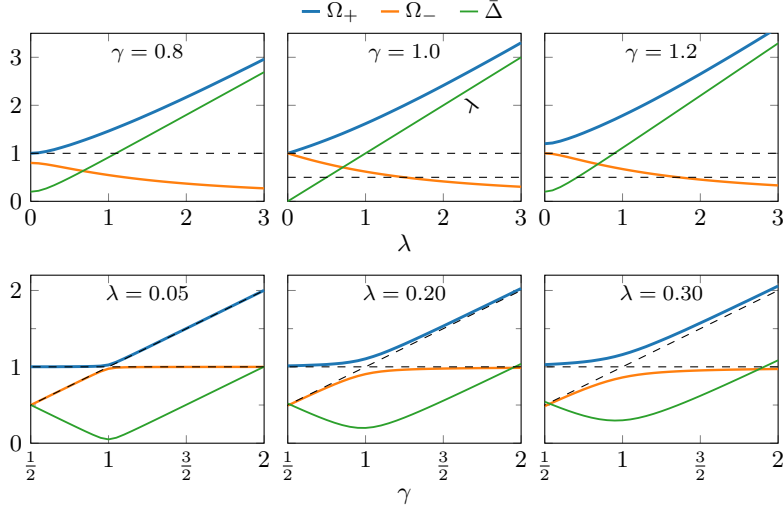


FIG. 11. Top panels – Polariton branches, Ω_{\pm} and VRS, $\bar{\Delta} \equiv \Omega_{+} - \Omega_{-}$ as a function of the collective coupling constant, λ . At resonance, $\bar{\Delta} = \lambda$. Bottom panels – Ω_{\pm} and $\bar{\Delta}$ as a function of γ . The functions' asymmetry about $\gamma = 1$ increases with λ .

$\hat{\mathbf{A}}$, and (ii) the term $\hat{H}_{2\text{deg-rel}}$ depends on the relative distances, decoupled from $\hat{\mathbf{A}}$. The two terms are given by

$$\begin{aligned} \hat{H}_{2\text{deg-cm}} &= \frac{1}{2m} \left(i\hbar \nabla_{\mathbf{R}} + e\hat{\mathbf{A}}_{\text{ext}}(\hat{\mathbf{R}}) + e\sqrt{N}\hat{\mathbf{A}} \right)^2 + \hbar\omega \left(\hat{a}^{\dagger}\hat{a} + \frac{1}{2} \right), \\ \hat{H}_{2\text{deg-rel}} &= \frac{1}{2m} \sum_{j=2}^N \left[\frac{i\hbar \tilde{\nabla}_j}{\sqrt{N}} + e\sqrt{N}\hat{\mathbf{A}}_{\text{ext}}(\hat{\mathbf{r}}_j) \right]^2 - \frac{\hbar^2}{2mN} \sum_{j,l=2}^N \tilde{\nabla}_j \cdot \tilde{\nabla}_l - \frac{e^2}{2m} \left[\sum_{j=2}^N \hat{\mathbf{A}}_{\text{ext}}(\hat{\mathbf{r}}_j) \right]^2 \\ &\quad + \sum_{1 < l}^N W(\sqrt{N}\hat{\mathbf{r}}_l) + \sum_{2 \leq i < l}^N W(\sqrt{N}(\hat{\mathbf{r}}_i - \hat{\mathbf{r}}_l)). \end{aligned} \quad (\text{A14})$$

Appendix B: Polariton Branches

This Appendix presents the polariton frequencies and their dependence on the collective coupling constant, λ and $\gamma \equiv \omega/\Omega$. Here, ω is the cavity mode frequency, and Ω is the harmonic matter trap frequency. The dimensionless upper/lower polariton frequencies are defined in Eq. (17) [53],

$$\Omega_{\pm}^2 = \frac{1 + \gamma^2 + \gamma\lambda^2}{2} \pm \frac{1}{2} \sqrt{(1 + \gamma^2 + \gamma\lambda^2)^2 - 4\gamma^2}, \quad (\text{B1})$$

where the collective coupling constant depends on the number of trapped particles, $N \geq 1$ as $\lambda \equiv \sqrt{Ng_0^2/(\pi\epsilon_0 c\mathcal{A}m\Omega)}$. Here, g_0 is the single particle coupling constant, \mathcal{A} is the area of the resonator mirror, m is the particle mass, ϵ_0 is the vacuum permittivity, c is the speed of light. Fig. 11 shows the λ, γ -dependence of Ω_{\pm} and VRS, $\bar{\Delta} \equiv (\Omega_{+} - \Omega_{-})$. Note that the asymmetry relative to the point $\gamma = 1$ increases with λ .

In the RWA, the terms proportional to $\lambda\hat{a}^{\dagger}\hat{b}^{\dagger}$, $\lambda\hat{a}\hat{b}$, and λ^2 in the Hamiltonian [see Eq. (15)] are omitted, and the polariton branches are given by

$$\Omega_{\text{RWA},\pm}^2 = \frac{1 + \gamma^2 + \lambda^2/2}{2} \pm \frac{1}{2} \sqrt{(\gamma + 1)^2[(\gamma - 1)^2 + \lambda^2]}. \quad (\text{B2})$$

Under the RWA, the VRS is symmetric relative to $\gamma = 1$. To verify this, it is sufficient to consider $\bar{\Delta}_{\text{RWA}}^2 = (\Omega_{\text{RWA},+} - \Omega_{\text{RWA},-})^2$, which is given by

$$\bar{\Delta}_{\text{RWA}}^2 = (\gamma - 1)^2 + \lambda^2; \quad \lambda^2 < 4\gamma. \quad (\text{B3})$$

Appendix C: Semiclassical Approach

The semiclassical approach relies on solving Hamilton's equations of motion derived from the classical counterpart of $\hat{\mathcal{H}}$ in Eq. (15)

$$\dot{X} = P - \lambda q, \quad \dot{P} = -X, \quad (\text{C1a})$$

$$\dot{q} = \gamma p, \quad \dot{p} = -\gamma q + \lambda P - \lambda^2 q. \quad (\text{C1b})$$

This system of linear differential equations can be solved by the Laplace transform method. Laplace transform, denoted by \mathcal{L} , turns the set of differential equations into a system of algebraic equations since $\mathcal{L}(\dot{f}) = \tilde{f}(s) - f(0)$, where $\tilde{f}(s)$ is the Laplace transform of f , s is the Laplace space variable, and $f(0)$ is the initial value of f . Solving the algebraic system yields,

$$\tilde{X}(s) = \frac{X(0)[s^3 + \gamma(\gamma + \lambda^2)s] + P(0)[s^2 + \gamma^2]}{h(s)} - \lambda s \frac{q(0)s + \gamma p(0)}{h(s)}, \quad (\text{C2a})$$

$$\tilde{P}(s) = \frac{[sP(0) - X(0)][s^2 + \gamma(\gamma + \lambda^2)]}{h(s)} + \lambda \frac{q(0)s + \gamma p(0)}{h(s)}, \quad (\text{C2b})$$

$$\tilde{q}(s) = \gamma \lambda s \frac{P(0) - X(0)}{h(s)} + (s^2 + 1) \frac{q(0)s + \gamma p(0)}{h(s)}, \quad (\text{C2c})$$

$$\tilde{p}(s) = \lambda s \frac{P(0)s - X(0)}{h(s)} - \frac{q(0)[\gamma + s^2(\gamma + \lambda^2)]}{h(s)} + \frac{p(0)(s^3 + s)}{h(s)}, \quad (\text{C2d})$$

where $h(s) = s^4 + s^2[\gamma(\gamma + \lambda^2) + 1] + \gamma^2$ is the characteristic polynomial of the linear system, and $X(0)$, $P(0)$, $q(0)$, and $p(0)$ are the initial values. The roots of $h(s)$ are given by $s_{1,2} = i\Omega_{\pm}$ and $s_{3,4} = -i\Omega_{\pm}$, where Ω_{\pm} are the upper/lower polariton frequencies in Eq. (B1). With those roots, $X(t)$, $P(t)$, $q(t)$ and $p(t)$ can be found by applying the inverse Laplace transform, \mathcal{L}^{-1} to Eqs. (C2a)-(C2d). The expectation values are obtained semiclassically by averaging the classical expression for an observable $\hat{O}(t)$, $O(t) = f[X(t), P(t), q(t), p(t)]$ with respect to the initial phase space distribution $\mathcal{P}(0)$

$$\langle \hat{O}(t) \rangle = \int \cdots \int_{-\infty}^{\infty} O(t) \mathcal{P}(0) d\mathbb{V}, \quad (\text{C3})$$

where $d\mathbb{V} \equiv dX(0)dP(0)dq(0)dp(0)$. The phase space distribution is derived from the initial wave function and thus accounts for the position-momentum uncertainty. For example, the wave function, $\psi_0(X, q) \propto \exp[-(X - X_0)^2/(2w^2)] \exp(-q^2/2)$ corresponds to the phase space distribution

$$\mathcal{P}(0) = \frac{1}{\pi^2} e^{-[X(0) - X_0]^2 w^{-2} - P(0)w^2} e^{-q^2(0) - p^2(0)}, \quad (\text{C4})$$

where X_0 is the initial displacement of the matter CM quadrature and w is the initial width of the state (for the decoupled CM ground state, $w = 1$).

1. Expectation Value of the Matter CM X Quadrature

In the case of $\langle \hat{X}(t) \rangle$, only the first term $\propto X(0)$ [see Eq. (C2a)] contributes to $X(t)$ after the integration in Eq. (C3). Simplification yields [same as Eq. (20)]

$$\frac{\langle \hat{X}(t) \rangle}{X_0} = \cos \left[\frac{\bar{\Sigma} t}{2} \right] \cos \left[\frac{\bar{\Delta} t}{2} \right] + \beta \sin \left[\frac{\bar{\Sigma} t}{2} \right] \sin \left[\frac{\bar{\Delta} t}{2} \right], \quad (\text{C5})$$

where $\bar{\Sigma} \equiv \Omega_+ + \Omega_-$, $\bar{\Delta} \equiv \Omega_+ - \Omega_-$ is the VRS ($\bar{\Sigma} < \bar{\Delta}$), and $\beta = (\Omega_+^2 + \Omega_-^2 - 2)/(\bar{\Sigma}\bar{\Delta})$. Under RWA,

$$\frac{\langle \hat{X}(t) \rangle_{\text{RWA}}}{X_0} = \cos \left[\frac{\bar{\Sigma}_{\text{RWA}} t}{2} \right] \cos \left[\frac{\bar{\Delta}_{\text{RWA}} t}{2} \right] + \beta_{\text{RWA}} \sin \left[\frac{\bar{\Sigma}_{\text{RWA}} t}{2} \right] \sin \left[\frac{\bar{\Delta}_{\text{RWA}} t}{2} \right], \quad (\text{C6})$$

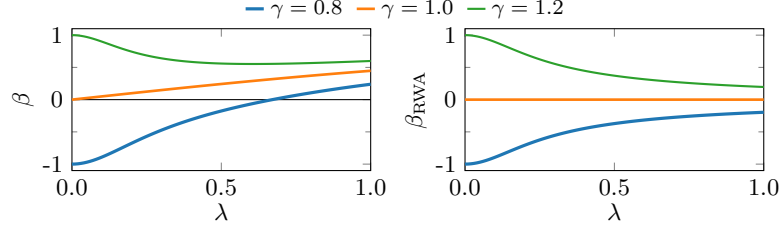


FIG. 12. Factors β and β_{RWA} in Eqs. (C5) and (C6). β_{RWA} vanishes at resonance, while $\beta(\gamma = 1)$ scales approximately linearly with λ (for $\lambda < 1$). Moreover, $|\beta|$ is sensitive to the sign of the relative detuning, $\gamma - 1$, while $|\beta_{\text{RWA}}|$ is not.

where $\bar{\Sigma}_{\text{RWA}}$, $\bar{\Delta}_{\text{RWA}}$, β_{RWA} are defined in terms of $\Omega_{\text{RWA},\pm}$.

β factor.—Fig. 12 compares β and β_{RWA} . While at resonance β scales approximately linearly with λ (for $\lambda < 1$), $\beta_{\text{RWA}}(\gamma = 1)$ vanishes. This suggests that the ultra-strong coupling effects in $\langle X(t) \rangle$, induced by CRT, are most emphasized at resonance.

Appendix D: Probability Density and Phase Space Distribution

In this section, we outline the semiclassical derivation of the exact matter CM probability density, $\mathcal{P}(X, t)$, and discuss its behavior in Scheme I (for shifted and squeezed matter initial state). Additionally, we discuss the general form of the matter and light phase space distributions. First, we invert $X[t; X(0)]$ to obtain $X(0)$ as a function of time and the rest of the initial conditions

$$X(0) = \frac{X(t) - f_2(t)P(0) - f_3(t)q(0) - f_4(t)p(0)}{f_1(t)}. \quad (\text{D1})$$

The time-dependent functions, $f_{1,\dots,4}$ are given by

$$f_1(t) = \langle \hat{X}(t) \rangle / X_0, \quad (\text{D2a})$$

$$f_2(t) = \frac{(\Omega_+^2 - \gamma^2) \sin(\Omega_+ t)}{\Omega_+ \bar{\Delta} \bar{\Sigma}} - \frac{(\Omega_-^2 - \gamma^2) \sin(\Omega_- t)}{\Omega_- \bar{\Delta} \bar{\Sigma}}, \quad (\text{D2b})$$

$$f_3(t) = -\lambda \frac{\Omega_+ \sin(\Omega_+ t) - \Omega_- \sin(\Omega_- t)}{\bar{\Delta} \bar{\Sigma}}, \quad (\text{D2c})$$

$$f_4(t) = \lambda \gamma \frac{\cos(\Omega_+ t) - \cos(\Omega_- t)}{\bar{\Delta} \bar{\Sigma}}. \quad (\text{D2d})$$

Substituting the obtained expression for $X(0)$ into the initial phase space distribution in Eq. (C4), and integrating out $P(0)$, $q(0)$, and $p(0)$, yields

$$\mathcal{P}(X, t) = \frac{\exp \left[-\frac{[X - f_1 X_0]^2}{w^2 f_1^2 + f_2^2/w^2 + f_3^2 + f_4^2} \right]}{\sqrt{\pi} \sqrt{w^2 f_1^2 + f_2^2/w^2 + f_3^2 + f_4^2}}. \quad (\text{D3})$$

It can be shown that

$$w^2 f_1^2 + f_2^2/w^2 + f_3^2 + f_4^2 = 2 \langle [\Delta \hat{X}(t)]^2 \rangle, \quad (\text{D4})$$

where $\langle [\Delta \hat{X}(t)]^2 \rangle \equiv \langle \hat{X}^2(t) \rangle - \langle \hat{X}(t) \rangle^2$. Thus,

$$\mathcal{P}(X, t) = \frac{1}{\sqrt{2\pi \langle [\Delta \hat{X}(t)]^2 \rangle}} \exp \left[-\frac{(X - \langle \hat{X}(t) \rangle)^2}{2 \langle [\Delta \hat{X}(t)]^2 \rangle} \right]. \quad (\text{D5})$$

Fig. 13(a,b) shows an example of $\mathcal{P}(X, t)$. The CM wave packet combines oscillatory and breathing motions about the mean. The wave packet width (variance) increases between the turning points, as seen in

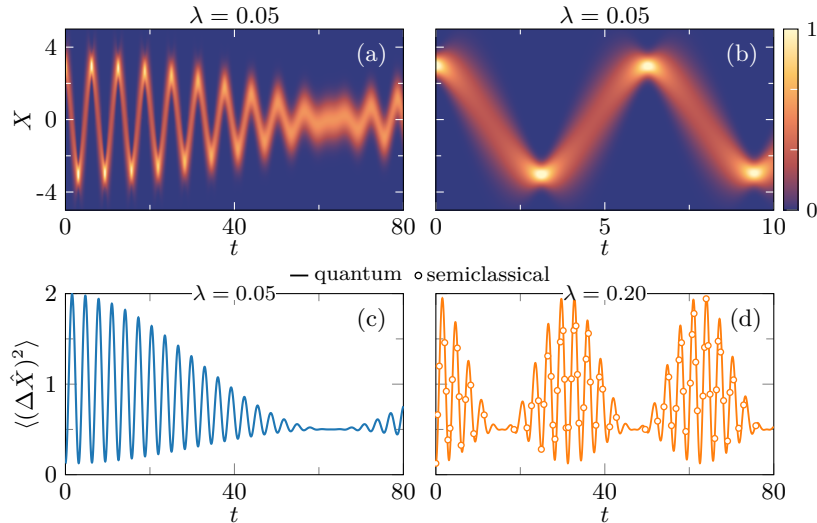


FIG. 13. (a,b) Matter CM quadrature probability density, $\mathcal{P}(X,t)$ in Eq. (D5). The wave packet motion combines oscillations and breathing about the mean value. The total probability is conserved, which causes the bright spots when the width of the wave packet is minimized. (c,d) Variance of $\mathcal{P}(X,t)$. Local minima are attained at the turning points of the wave packet, i.e., at the extrema of $\langle\hat{X}(t)\rangle$. Parameters: $\gamma = 1$, $X_0 = 3$, $w = 0.5$.

Fig. 13(b). The bright spots in the density plots appear when the width is minimum, since the amplitude is maximized at those moments to conserve the total probability.

Phase space distributions.—Generally, phase space distributions of both matter and light subsystems are multivariate (two-dimensional) Gaussians. A Gaussian function in two dimensions (X and P , or q and p) depends on six parameters, the coordinates of the center [$\mu_{X,P}(t)$ or $\mu_{q,p}(t)$], and the elements of the covariance matrix

$$\Sigma(t) = \begin{bmatrix} \sigma_X^2(t) & \sigma_{XP}(t) \\ \sigma_{XP}(t) & \sigma_P^2(t) \end{bmatrix} \quad \text{or} \quad \Sigma(t) = \begin{bmatrix} \sigma_q^2(t) & \sigma_{qp}(t) \\ \sigma_{qp}(t) & \sigma_p^2(t) \end{bmatrix}. \quad (\text{D6})$$

For example, the photon phase space distribution is given by

$$\mathcal{P}(q,p,t) = \frac{1}{2\pi\sqrt{\sigma_q^2\sigma_p^2 - \sigma_{qp}^2}} \exp\left[-\frac{\sigma_p^2(q - \mu_q)^2}{2(\sigma_q^2\sigma_p^2 - \sigma_{qp}^2)}\right] \exp\left[-\frac{\sigma_q^2(p - \mu_p)^2}{2(\sigma_q^2\sigma_p^2 - \sigma_{qp}^2)} + \frac{2\sigma_{qp}(q - \mu_q)(p - \mu_p)}{2(\sigma_q^2\sigma_p^2 - \sigma_{qp}^2)}\right], \quad (\text{D7})$$

where $\sigma_\nu^2 \equiv \langle(\Delta\hat{\nu})^2\rangle = \langle\hat{\nu}^2\rangle - \mu_\nu^2$, $\sigma_{qp} \equiv \langle(\Delta\hat{q}\hat{p})\rangle = \langle\hat{q}\hat{p}\rangle - \mu_q\mu_p$, and $\mu_\nu \equiv \langle\hat{\nu}\rangle$ ($\nu = q, p$). Phase space distribution such as in Eq. (D7) appear as rotated ellipses centered around (μ_q, μ_p) . The eigenvectors of the covariance matrix define the orientation of the ellipses, while the aspect ratio is proportional to the ratio of the eigenvalues.

Higher-order expectation values related to the matter or light subsystems can be conveniently obtained by averaging the corresponding classical expressions with respect to the phase space distributions. The higher-order averages over a two-dimensional Gaussian distribution are entirely determined by the distribution's first two moments, namely the means [e.g., $\mu_{X,P}(t)$ or $\mu_{q,p}(t)$] and the elements of Σ .

Appendix E: Photon Number Expectation Value

In this section, we explore the properties of photon number expectation value in Schemes I and II. In both cases, we consider the RWA, allowing us to isolate the ultrastrong-coupling effects arising from the counter-rotating and diamagnetic terms of the Hamiltonian.

1. Scheme I

Using the phase space distribution in Eq. (D7) the expectation value of the photon number $\hat{n} = \hat{a}^\dagger \hat{a} = (\hat{q}^2 + \hat{p}^2)/2 - 1/2$ can be conveniently found by following the semiclassical approach outlined in Sec. C. To simplify the expression, we subtract the relatively small average photon number when the CM is in the ground state. Thus, the considered quantity is $\Delta \langle \hat{n}(t) \rangle \equiv \langle \hat{n}(t) \rangle - \langle \hat{n}(t; X_0 = 0, w = 1) \rangle$, which is given by

$$\begin{aligned} \Delta \langle \hat{n}(t) \rangle = & \lambda^2 (w^{-2} - 1) \left(\frac{\gamma^2 \sin^2(\bar{\Sigma}t/2) \sin^2(\bar{\Delta}t/2)}{\bar{\Sigma}^2 \bar{\Delta}^2} + \frac{[\Omega_+ \sin(\bar{\Sigma}t/2) \cos(\bar{\Delta}t/2) - (\bar{\Sigma}/2) \sin(\Omega_- t)]^2}{\bar{\Sigma}^2 \bar{\Delta}^2} \right) \\ & + \lambda^2 (2X_0^2 + w^2 - 1) \left(\gamma^2 \frac{[\Omega_- \sin(\bar{\Sigma}t/2) \cos(\bar{\Delta}t/2) - (\bar{\Sigma}/2) \sin(\Omega_- t)]^2}{\Omega_+^2 \Omega_-^2 \bar{\Sigma}^2 \bar{\Delta}^2} + \frac{\sin^2(\bar{\Sigma}t/2) \sin^2(\bar{\Delta}t/2)}{\bar{\Sigma}^2 \bar{\Delta}^2} \right), \end{aligned} \quad (\text{E1})$$

The time-averaged value reads

$$\Delta \overline{\langle \hat{n} \rangle} = \lambda^2 (w^{-2} - 1) f_1 + \lambda^2 (2X_0^2 + w^2 - 1) f_2, \quad (\text{E2})$$

where $f_{1,2}$ [see Eq. (21)] are defined as

$$f_1 = \frac{\Omega_+^2 + \Omega_-^2 + 2\gamma^2}{8\bar{\Sigma}^2 \bar{\Delta}^2} = \frac{1}{8} \frac{\gamma(3\gamma + \lambda^2) + 1}{\gamma^2[(\gamma + \lambda^2)^2 - 2] + 2\gamma\lambda^2 + 1}, \quad (\text{E3a})$$

$$f_2 = \frac{2\Omega_+^2 \Omega_-^2 + \gamma^2(\Omega_+^2 + \Omega_-^2)}{8\Omega_+^2 \Omega_-^2 \bar{\Sigma}^2 \bar{\Delta}^2} = \frac{1}{8} \frac{\gamma(\gamma + \lambda^2) + 3}{\gamma^2[(\gamma + \lambda^2)^2 - 2] + 2\gamma\lambda^2 + 1}. \quad (\text{E3b})$$

At resonance, $f_{1,2}$ simplify to $f_1 = f_2 = 1/(8\lambda^2)$, and $\Delta \overline{\langle \hat{n} \rangle}$ becomes independent of λ ,

$$\Delta \overline{\langle \hat{n}(\gamma = 1) \rangle} = \frac{X_0^2}{4} + \frac{1}{8} (w - w^{-1})^2. \quad (\text{E4})$$

When $w \sim 1$, $\Delta \overline{\langle \hat{n} \rangle}$ can be roughly estimated by the single term proportional to X_0^2 ,

$$\Delta \overline{\langle \hat{n} \rangle} \approx X_0^2 \cdot (2\lambda^2 f_2). \quad (\text{E5})$$

Fig. 5(a,b) shows $\Delta \overline{\langle \hat{n} \rangle}$ as a function of λ and γ . In panel (b), the asymmetry about the point of resonance, $\gamma = 1$ increases with λ . Next, by comparison with the RWA, we demonstrate that the asymmetry stems from the ultrastrong coupling and CRT.

Rotating Wave Approximation.—In the RWA, the Hamiltonian takes the form

$$\hat{\mathcal{H}}_{\text{RWA}} = \left[\hat{b}^\dagger \hat{b} + \frac{1}{2} \right] + \gamma \left[\hat{a}^\dagger \hat{a} + \frac{1}{2} \right] - i \frac{\lambda}{2} \hat{b}^\dagger \hat{a} + i \frac{\lambda}{2} \hat{b} \hat{a}^\dagger. \quad (\text{E6})$$

Expressing $\hat{\mathcal{H}}_{\text{RWA}}$ in terms of \hat{X} , \hat{P} , \hat{q} , and \hat{p} , and following the semiclassical approach, we can obtain the photon number expectation value

$$\begin{aligned} \langle \hat{n}(t) \rangle_{\text{RWA}} = & \lambda^2 [2X_0^2 + (w - w^{-1})^2] \frac{(\gamma + 1)^2 \sin^2(\bar{\Sigma}_{\text{RWA}} t/2) \sin^2(\bar{\Delta}_{\text{RWA}} t/2)}{4\bar{\Sigma}_{\text{RWA}}^2 \bar{\Delta}_{\text{RWA}}^2} + \lambda^2 [2X_0^2 + (w - w^{-1})^2] \\ & \times \frac{[\Omega_{\text{RWA},-}(\gamma - \lambda^2/4 + \Omega_{\text{RWA},+}^2) \sin(\Omega_{\text{RWA},+} t) - \Omega_{\text{RWA},+}(\gamma - \lambda^2/4 + \Omega_{\text{RWA},-}^2) \sin(\Omega_{\text{RWA},-} t)]^2}{16\Omega_{\text{RWA},+}^2 \Omega_{\text{RWA},-}^2 \bar{\Sigma}_{\text{RWA}}^2 \bar{\Delta}_{\text{RWA}}^2}, \end{aligned} \quad (\text{E7})$$

where $\Omega_{\text{RWA},\pm}$ are defined in Eq. (B2). Note that in the full system, $\overline{\langle \hat{n} \rangle}$ differs from zero for the CM ground state ($X_0 = 0, w = 1$). That is why we defined $\Delta \langle \hat{n}(t) \rangle$ in Eq. (E1) to simplify the analysis. In contrast, under RWA, $\langle \hat{n}(t; X_0 = 0, w = 1) \rangle \equiv 0$ as seen from Eq. (E7). The time average of $\langle \hat{n}(t) \rangle_{\text{RWA}}$ is given by the simple expression

$$\overline{\langle \hat{n} \rangle}_{\text{RWA}} = \frac{1}{8} \frac{\lambda^2}{(\gamma - 1)^2 + \lambda^2} [2X_0^2 + (w - w^{-1})^2]. \quad (\text{E8})$$

At resonance ($\gamma = 1$), $\overline{\langle \hat{n} \rangle}_{\text{RWA}}$ reduces to Eq. (E4). Under RWA, the prefactor of X_0^2 (in this case, it is the overall prefactor) is a Lorentzian function of γ of width λ centered at $\gamma = 1$,

$$2\lambda^2 f_{\text{RWA}} = \frac{1}{4} \frac{\lambda^2}{(\gamma - 1)^2 + \lambda^2}. \quad (\text{E9})$$

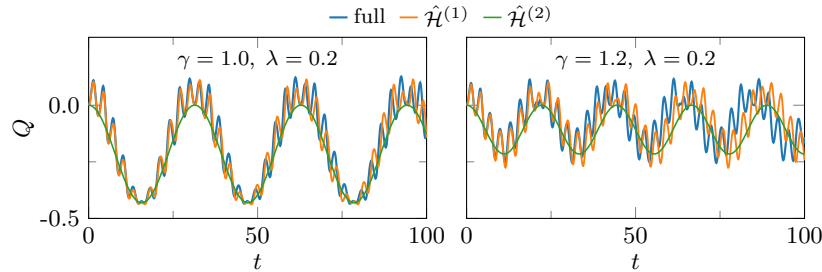


FIG. 14. Photon Q function in Scheme I obtained by direct numerical solution of the Schrödinger equation with the HH in Eq. (15) vs $\hat{\mathcal{H}}^{(1,2)}$ in Eqs. (F4) and (F5). Initial matter state parameters: $X_0 = 3$, $w = 0.5$.

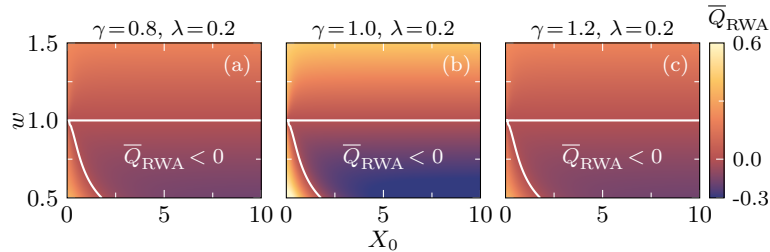


FIG. 15. The dependence of photon \bar{Q} on the initial displacement and width of the matter CM X quadrature under RWA. In contrast to Fig. 6(c-e), the pictures on either side of the resonance are identical here.

Appendix F: Mandel Q function

The first subsection presents the analytical expression for the *initial* Q function in the matter subsystem in Scheme I. The following subsections discuss the impact of the diamagnetic term and the RWA on Q .

1. Initial Q_{mat} Function in Scheme I

To obtain the analytical expression for the initial Mandel Q function of the matter state, $Q_{\text{mat}}(0)$ in Scheme I (i.e., for a shifted by X_0 and squeezed Gaussian), we use the formulas for $\langle \hat{n} \rangle$ and $\langle (\Delta \hat{n})^2 \rangle$ in Eqs. (7.100) and (7.102) in [83]

$$\langle \hat{n} \rangle = |\alpha|^2 + \sinh^2 r, \quad \langle (\Delta \hat{n})^2 \rangle = |\alpha|^2 e^{2r} + 2 \sinh^2 r \cosh^2 r. \quad (\text{F1})$$

For the considered Gaussian initial state, $|\alpha|^2 = X_0^2/2$ and $r = -\ln(w)$. Substitution yields

$$Q_{\text{mat}}(0) \equiv \frac{\langle (\Delta \hat{n})^2 \rangle - \langle \hat{n} \rangle}{\langle \hat{n} \rangle} = \frac{(w^2 - 1)^2(w^4 + 1) + 4w^4(w^2 - 1)X_0^2}{4w^4X_0^2 + 2w^2(w^2 - 1)^2}. \quad (\text{F2})$$

Expanding in powers of X_0^{-2} , yields

$$Q_{\text{mat}}(0) = (w^2 - 1) - \frac{(w^2 - 1)^2(w^4 - 2w^2 - 1)}{4w^4X_0^2} + \mathcal{O}(X_0^{-4}). \quad (\text{F3})$$

Thus, we obtain the expression used in the main text, $Q_{\text{mat}}(0) = (w^2 - 1)[1 + \mathcal{O}(X_0^{-2})]$.

2. Diamagnetic Term and RWA in Scheme I

For an initially squeezed matter CM state, the photon Q function may attain negative values even in the absence of the diamagnetic term proportional to λ^2 i.e., with the Hamiltonian

$$\hat{\mathcal{H}}^{(1)} = \left[\hat{b}^\dagger \hat{b} + \frac{1}{2} \right] + \gamma \left[\hat{a}^\dagger \hat{a} + \frac{1}{2} \right] - i \frac{\lambda}{2} (\hat{b}^\dagger - \hat{b})(\hat{a}^\dagger + \hat{a}). \quad (\text{F4})$$

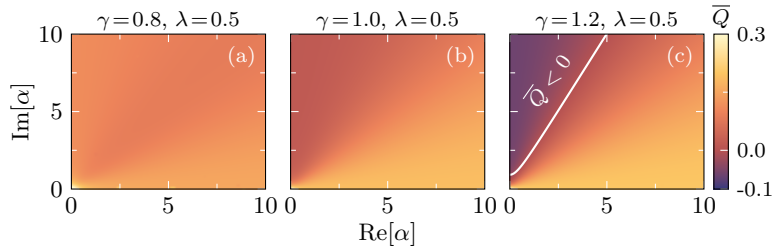


FIG. 16. The dependence of photon \bar{Q} on the initial coherent state of the cavity field. Sub-Poissonian PND is achieved off-resonance, and the effect is sensitive to the phase of α . In the ultra-strong coupling regime here, $\bar{Q} < 0$ is completely absent in the red-shifted cavity. The negativity saturates with an increasing imaginary component of α .

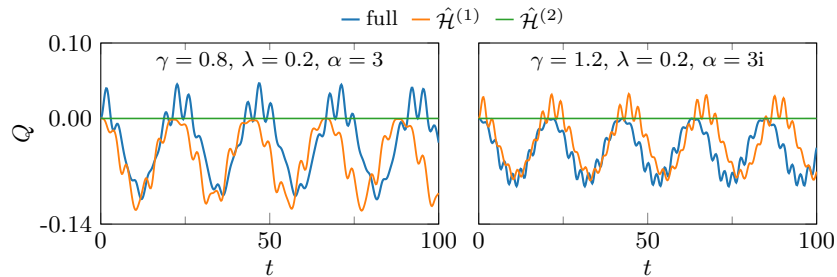


FIG. 17. Photon $Q(t)$ function in Scheme II obtained by direct numerical solution of the Schrödinger equation with the HH in Eq. (15) vs $\hat{\mathcal{H}}^{(1,2)}$ in Eqs. (F4) and (F5).

Under the RWA, i.e., with the Hamiltonian

$$\hat{\mathcal{H}}^{(2)} = \left[\hat{b}^\dagger \hat{b} + \frac{1}{2} \right] + \gamma \left[\hat{a}^\dagger \hat{a} + \frac{1}{2} \right] - i \frac{\lambda}{2} \hat{b}^\dagger \hat{a} + i \frac{\lambda}{2} \hat{b} \hat{a}^\dagger, \quad (\text{F5})$$

the effective transfer of nonclassical matter state into the cavity mode is still possible. Fig. 14 compares the photon Q functions obtained with the HH vs $\hat{\mathcal{H}}^{(1,2)}$. To isolate the ultrastrong coupling effect, we reproduce Fig. 6(c-e) in Fig. 15 but under RWA Hamiltonian. \bar{Q}_{RWA} is insensitive to the sign of the relative detuning $(\gamma - 1)$, i.e., panels (a) and (c) are identical. In contrast, panels (c) and (e) in Fig. 6 exhibit asymmetry induced by the terms omitted in the RWA.

3. Diamagnetic Term and RWA in Scheme II

Fig. 16 shows additional examples of the constant component of the photon Q function, \bar{Q} in Scheme II for a range of initial coherent states of the cavity, $|\alpha\rangle$. In this example of the ultra-strong coupling regime,

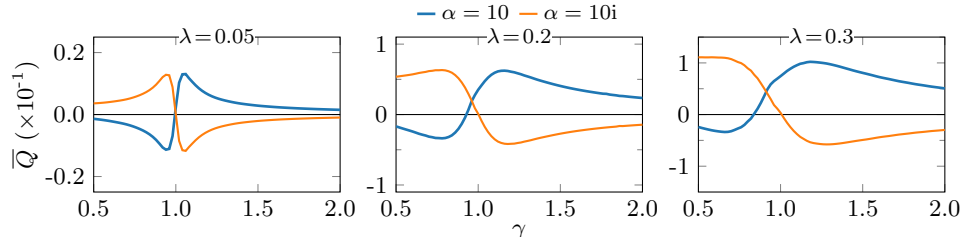


FIG. 18. Dependence of the constant component of the photon Q function, \bar{Q} on γ for real/imaginary α , defining the initial coherent state, $|\alpha\rangle$. The chosen values of α are sufficiently high so that \bar{Q} is saturated and no longer changes with increasing α .

the asymmetry between the red and blue shifted cavities is so pronounced that negative \overline{Q} is obtained only on one side, for $\gamma = 1.2$.

The coherent initial state of the cavity used in Scheme II is not squeezed, i.e., $Q(t=0) = 0$. Therefore, the counter-rotating terms are essential for generating squeezing and achieving $Q < 0$. Fig. 17 shows that under the RWA [i.e., with $\hat{\mathcal{H}}^{(2)}$ in Eq. (F5)], Q remains zero throughout the motion. In contrast, neglecting the diamagnetic terms [i.e., with $\hat{\mathcal{H}}^{(1)}$ in Eq. (F4)] produce qualitatively similar results to the full Hamiltonian with negative (on average) photon Q function. Fig. 18 focuses on the asymmetry of \overline{Q} about the point of resonance ($\gamma = 1$). Consistent with Fig. 9, the asymmetry between initial coherent states, $|\alpha\rangle$ with real or imaginary α increases with λ .

-
- [1] I. Carusotto and C. Ciuti, Quantum fluids of light, *Rev. Mod. Phys.* **85**, 299 (2013).
 - [2] A. Frisk Kockum, A. Miranowicz, S. De Liberato, S. Savasta, and F. Nori, Ultrastrong coupling between light and matter, *Nat. Rev. Phys.* **1**, 19 (2019).
 - [3] P. Forn-Díaz, L. Lamata, E. Rico, J. Kono, and E. Solano, Ultrastrong coupling regimes of light-matter interaction, *Rev. Mod. Phys.* **91**, 025005 (2019).
 - [4] D. N. Basov, A. Asenjo-Garcia, P. J. Schuck, X. Zhu, and A. Rubio, Polariton panorama, *Nanophotonics* **10**, 549 (2021).
 - [5] F. Appugliese, J. Enkner, G. L. Paravicini-Bagliani, M. Beck, C. Reichl, W. Wegscheider, G. Scalari, C. Ciuti, and J. Faist, Breakdown of topological protection by cavity vacuum fields in the integer quantum Hall effect, *Science* **375**, 1030 (2022).
 - [6] J. Enkner, L. Graziotto, F. Appugliese, V. Rokaj, J. Wang, M. Ruggenthaler, C. Reichl, W. Wegscheider, A. Rubio, and J. Faist, Testing the Renormalization of the von Klitzing Constant by Cavity Vacuum Fields, *Phys. Rev. X* **14**, 021038 (2024).
 - [7] D. Hagenmüller, S. De Liberato, and C. Ciuti, Ultrastrong coupling between a cavity resonator and the cyclotron transition of a two-dimensional electron gas in the case of an integer filling factor, *Phys. Rev. B* **81**, 235303 (2010).
 - [8] G. Scalari, C. Maissen, D. Turčinková, D. Hagenmüller, S. D. Liberato, C. Ciuti, C. Reichl, D. Schuh, W. Wegscheider, M. Beck, and J. Faist, Ultrastrong Coupling of the Cyclotron Transition of a 2D Electron Gas to a THz Metamaterial, *Science* **335**, 1323 (2012).
 - [9] A. Bayer, M. Pozimski, S. Schambeck, D. Schuh, R. Huber, D. Bougeard, and C. Lange, Terahertz Light-Matter Interaction beyond Unity Coupling Strength, *Nano Lett.* **17**, 6340 (2017).
 - [10] S. Ravets, P. Knüppel, S. Faelt, O. Cotlet, M. Kroner, W. Wegscheider, and A. Imamoğlu, Polaron Polaritons in the Integer and Fractional Quantum Hall Regimes, *Phys. Rev. Lett.* **120**, 057401 (2018).
 - [11] M. A. Sentef, M. Ruggenthaler, and A. Rubio, Cavity quantum-electrodynamical polaritonically enhanced electron-phonon coupling and its influence on superconductivity, *Sci. Adv.* **4**, eaau6969 (2018).
 - [12] X. Li, M. Bamba, Q. Zhang, S. Fallahi, G. C. Gardner, W. Gao, M. Lou, K. Yoshioka, M. J. Manfra, and J. Kono, Vacuum Bloch-Siegert shift in Landau polaritons with ultra-high cooperativity, *Nature Photon.* **12**, 324 (2018).
 - [13] F. Schlawin, A. Cavalleri, and D. Jaksch, Cavity-Mediated Electron-Photon Superconductivity, *Phys. Rev. Lett.* **122**, 133602 (2019).
 - [14] J. B. Curtis, Z. M. Raines, A. A. Allocca, M. Hafezi, and V. M. Galitski, Cavity Quantum Eliashberg Enhancement of Superconductivity, *Phys. Rev. Lett.* **122**, 167002 (2019), 1805.01482.
 - [15] V. Rokaj, J. Wang, J. Sous, M. Penz, M. Ruggenthaler, and A. Rubio, Weakened Topological Protection of the Quantum Hall Effect in a Cavity, *Phys. Rev. Lett.* **131**, 196602 (2023).
 - [16] F. Schlawin, D. M. Kennes, and M. A. Sentef, Cavity quantum materials, *Appl. Phys. Rev.* **9**, 011312 (2022).
 - [17] J. Kasprzak, M. Richard, S. Kundermann, A. Baas, P. Jeambrun, J. M. J. Keeling, F. M. Marchetti, M. H. Szymańska, R. André, J. L. Staehli, V. Savona, P. B. Littlewood, B. Deveaud, and L. S. Dang, Bose-Einstein condensation of exciton polaritons, *Nature* **443**, 409 (2006).
 - [18] Y. O. Dudin and A. Kuzmich, Strongly Interacting Rydberg Excitations of a Cold Atomic Gas, *Science* **336**, 887 (2012).
 - [19] T. Peyronel, O. Firstenberg, Q.-Y. Liang, S. Hofferberth, A. V. Gorshkov, T. Pohl, M. D. Lukin, and V. Vuletić, Quantum nonlinear optics with single photons enabled by strongly interacting atoms, *Nature* **488**, 57 (2012).
 - [20] F. Mivehvar, F. Piazza, T. Donner, and H. Ritsch, Cavity QED with quantum gases: new paradigms in many-body physics, *Adv. Phys.* **70**, 1 (2021).
 - [21] J. A. Hutchison, T. Schwartz, C. Genet, E. Devaux, and T. W. Ebbesen, Modifying Chemical Landscapes by

- Coupling to Vacuum Fields, *Angew. Chem.* **51**, 1592 (2012).
- [22] T. W. Ebbesen, Hybrid Light-Matter States in a Molecular and Material Science Perspective, *Acc. Chem. Res.* **49**, 2403 (2016).
- [23] J. George, T. Chervy, A. Shalabney, E. Devaux, H. Hiura, C. Genet, and T. W. Ebbesen, Multiple Rabi Splittings under Ultrastrong Vibrational Coupling, *Phys. Rev. Lett.* **117**, 153601 (2016).
- [24] P.-Y. Yang and J. Cao, Quantum effects in chemical reactions under polaritonic vibrational strong coupling, *J. Phys. Chem. Lett.* **12**, 9531 (2021).
- [25] A. Wu, J. Cerrillo, and J. Cao, Extracting kinetic information from short-time trajectories: relaxation and disorder of lossy cavity polaritons, *Nanophotonics* **13**, 2575 (2024).
- [26] D. Sidler, M. Ruggenthaler, C. Schäfer, E. Ronca, and A. Rubio, A perspective on *ab initio* modeling of polaritonic chemistry: The role of non-equilibrium effects and quantum collectivity, *J. Chem. Phys.* **156**, 230901 (2022).
- [27] J. Feist, J. Galego, and F. J. Garcia-Vidal, Polaritonic Chemistry with Organic Molecules, *ACS Photonics* **5**, 205 (2018).
- [28] S. Hou, M. Khatoniari, K. Ding, Y. Qu, A. Napolov, V. M. Menon, and S. R. Forrest, Ultralong-Range Energy Transport in a Disordered Organic Semiconductor at Room Temperature Via Coherent Exciton-Polariton Propagation, *Adv. Mater.* **32**, 2002127 (2020).
- [29] J. Keeling and S. Kéna-Cohen, Bose-Einstein Condensation of Exciton-Polaritons in Organic Microcavities, *Annu. Rev. Phys. Chem.* **71**, 435 (2020).
- [30] F. J. Garcia-Vidal, C. Ciuti, and T. W. Ebbesen, Manipulating matter by strong coupling to vacuum fields, *Science* **373**, eabd0336 (2021).
- [31] M. Balasubrahmaniam, A. Simkhovich, A. Golombek, G. Sandik, G. Ankonina, and T. Schwartz, From enhanced diffusion to ultrafast ballistic motion of hybrid light-matter excitations, *Nat. Mat.* **22**, 338 (2023).
- [32] J. A. Hutchison, A. Liscio, T. Schwartz, A. Canaguier-Durand, C. Genet, V. Palermo, P. Samorì, and T. W. Ebbesen, Tuning the Work Function Via Strong Coupling, *Adv. Mater.* **25**, 2481 (2013).
- [33] K. Sun and R. F. Ribeiro, Theoretical formulation of chemical equilibrium under vibrational strong coupling, *Nat. Commun.* **15**, 2405 (2024).
- [34] B. Xiang and W. Xiong, Molecular Polaritons for Chemistry, Photonics and Quantum Technologies, *Chem. Rev.* **124**, 2512 (2024).
- [35] T. Freixanet, B. Sermage, A. Tiberj, and R. Planel, In-plane propagation of excitonic cavity polaritons, *Phys. Rev. B* **61**, 7233 (2000).
- [36] E. Orgiu, J. George, J. A. Hutchison, E. Devaux, J. F. Dayen, B. Doudin, F. Stellacci, C. Genet, J. Schachenmayer, C. Genes, G. Pupillo, P. Samorì, and T. W. Ebbesen, Conductivity in organic semiconductors hybridized with the vacuum field, *Nat. Mater.* **14**, 1123 (2015).
- [37] R. Pandya, R. Y. S. Chen, Q. Gu, J. Sung, C. Schnedermann, O. S. Ojambati, R. Chikkaraddy, J. Gorman, G. Jacucci, O. D. Onelli, T. Willhammar, D. N. Johnstone, S. M. Collins, P. A. Midgley, F. Auras, T. Baikie, R. Jayaprakash, F. Mathevet, R. Soucek, M. Du, A. M. Alvertis, A. Ashoka, S. Vignolini, D. G. Lidzey, J. J. Baumberg, R. H. Friend, T. Barisien, L. Legrand, A. W. Chin, J. Yuen-Zhou, S. K. Saikin, P. Kukura, A. J. Musser, and A. Rao, Microcavity-like exciton-polaritons can be the primary photoexcitation in bare organic semiconductors, *Nat. Commun.* **12**, 6519 (2021).
- [38] G. Engelhardt and J. Cao, Unusual dynamical properties of disordered polaritons in microcavities, *Phys. Rev. B* **105**, 064205 (2022); Polariton localization and dispersion properties of disordered quantum emitters in multimode microcavities, *Phys. Rev. Lett.* **130**, 213602 (2023).
- [39] I. Sokolovskii, R. H. Tichauer, D. Morozov, J. Feist, and G. Groenhof, Multi-scale molecular dynamics simulations of enhanced energy transfer in organic molecules under strong coupling, *Nat. Commun.* **14**, 6613 (2023).
- [40] G. J. R. Aroeira, K. T. Kairys, and R. F. Ribeiro, Coherent transient exciton transport in disordered polaritonic wires, *Nanophotonics* **13**, 2553 (2024).
- [41] Z. Zhou, H.-T. Chen, M. Sukharev, J. E. Subotnik, and A. Nitzan, Nature of polariton transport in a Fabry-Perot cavity, *Phys. Rev. A* **109**, 033717 (2024).
- [42] G. Sandik, J. Feist, F. J. García-Vidal, and T. Schwartz, Cavity-enhanced energy transport in molecular systems, *Nat. Mater.* (2024).
- [43] M. Förg, L. Colombier, R. K. Patel, J. Lindlau, A. D. Mohite, H. Yamaguchi, M. M. Glazov, D. Hunger, and A. Högele, Cavity-control of interlayer excitons in van der Waals heterostructures, *Nat. Commun.* **10**, 3697 (2019).
- [44] S. Latini, E. Ronca, U. De Giovannini, H. Hübener, and A. Rubio, Cavity Control of Excitons in Two-Dimensional Materials, *Nano Lett.* **19**, 3473 (2019).
- [45] A. Kuhn, M. Hennrich, and G. Rempe, Deterministic Single-Photon Source for Distributed Quantum Networking, *Phys. Rev. Lett.* **89**, 067901 (2002).
- [46] U. L. Andersen, T. Gehring, C. Marquardt, and G. Leuchs, 30 years of squeezed light generation, *Phys. Scr.* **91**,

- 053001 (2016).
- [47] C. K. Law, Interaction between a moving mirror and radiation pressure: A Hamiltonian formulation, *Phys. Rev. A* **51**, 2537 (1995).
- [48] M. Aspelmeyer, T. J. Kippenberg, and F. Marquardt, Cavity optomechanics, *Rev. Mod. Phys.* **86**, 1391 (2014).
- [49] A. H. Safavi-Naeini, S. Gröblacher, J. T. Hill, J. Chan, M. Aspelmeyer, and O. Painter, Squeezed light from a silicon micromechanical resonator, *Nature* **500**, 185 (2013).
- [50] T. P. Purdy, P.-L. Yu, R. W. Peterson, N. S. Kampel, and C. A. Regal, Strong Optomechanical Squeezing of Light, *Phys. Rev. X* **3**, 031012 (2013).
- [51] D. W. C. Brooks, T. Botter, S. Schreppler, T. P. Purdy, N. Brahm, and D. M. Stamper-Kurn, Non-classical light generated by quantum-noise-driven cavity optomechanics, *Nature* **488**, 476 (2012).
- [52] H. Takahashi, E. Kassa, C. Christoforou, and M. Keller, Strong coupling of a single ion to an optical cavity, *Phys. Rev. Lett.* **124**, 013602 (2020).
- [53] V. Rokaj, S. I. Mistakidis, and H. R. Sadeghpour, Cavity induced collective behavior in the polaritonic ground state, *SciPost Phys.* **14**, 167 (2023).
- [54] J. J. Hopfield, Theory of the contribution of excitons to the complex dielectric constant of crystals, *Phys. Rev.* **112**, 1555 (1958).
- [55] V. Rokaj, D. M. Welakuh, M. Ruggenthaler, and A. Rubio, Light-matter interaction in the long-wavelength limit: no ground-state without dipole self-energy, *J. Phys. B: At. Mol. Opt. Phys.* **51**, 034005 (2018).
- [56] H. Spohn, *Dynamics of Charged Particles and their Radiation Field* (Cambridge University Press, Cambridge, UK, 2004).
- [57] A. Kreuter, C. Becher, G. P. T. Lancaster, A. B. Mundt, C. Russo, H. Häffner, C. Roos, J. Eschner, F. Schmidt-Kaler, and R. Blatt, Spontaneous Emission Lifetime of a Single Trapped Ca^+ Ion in a High Finesse Cavity, *Phys. Rev. Lett.* **92**, 203002 (2004).
- [58] A. Stute, B. Casabone, B. Brandstätter, D. Habicher, H. G. Barros, P. O. Schmidt, T. E. Northup, and R. Blatt, Toward an ion-photon quantum interface in an optical cavity, *Appl. Phys. B* **107**, 1145 (2012).
- [59] H. Takahashi, E. Kassa, C. Christoforou, and M. Keller, Cavity-induced anticorrelated photon-emission rates of a single ion, *Phys. Rev. A* **96**, 023824 (2017).
- [60] M. Keller, Cavity-QED with single trapped ions, *Contemp. Phys.* **63**, 1 (2022).
- [61] G. R. Guthöhrlein, M. Keller, K. Hayasaka, W. Lange, and H. Walther, A single ion as a nanoscopic probe of an optical field, *Nature* **414**, 49 (2001).
- [62] D. M. Meekhof, C. Monroe, B. E. King, W. M. Itano, and D. J. Wineland, Generation of nonclassical motional states of a trapped atom, *Phys. Rev. Lett.* **76**, 1796 (1996).
- [63] A. Stute, B. Casabone, B. Brandstätter, K. Friebe, T. E. Northup, and R. Blatt, Quantum-state transfer from an ion to a photon, *Nat. Photonics* **7**, 219 (2013).
- [64] A. D. Boozer, A. Boca, R. Miller, T. E. Northup, and H. J. Kimble, Reversible state transfer between light and a single trapped atom, *Phys. Rev. Lett.* **98**, 193601 (2007).
- [65] D. A. Hite, Y. Colombe, A. C. Wilson, D. T. C. Allcock, D. Leibfried, D. J. Wineland, and D. P. Pappas, Surface science for improved ion traps, *MRS Bulletin* **38**, 826 (2013).
- [66] S. Smolka, W. Wuester, F. Haupt, S. Faelt, W. Wegscheider, and A. Imamoğlu, Cavity quantum electrodynamics with many-body states of a two-dimensional electron gas, *Science* **346**, 332 (2014).
- [67] G. L. Paravicini-Bagliani, F. Appugliese, E. Richter, F. Valmorra, J. Keller, M. Beck, N. Bartolo, C. Rössler, T. Ihn, K. Ensslin, C. Ciuti, G. Scalari, and J. Faist, Magneto-transport controlled by Landau polariton states, *Nature Phys.* **15**, 186 (2019).
- [68] J. Keller, G. Scalari, F. Appugliese, S. Rajabali, M. Beck, J. Haase, C. A. Lehner, W. Wegscheider, M. Failla, M. Myronov, D. R. Leadley, J. Lloyd-Hughes, P. Nataf, and J. Faist, Landau polaritons in highly nonparabolic two-dimensional gases in the ultrastrong coupling regime, *Phys. Rev. B* **101**, 075301 (2020).
- [69] V. Rokaj, M. Penz, M. A. Sentef, M. Ruggenthaler, and A. Rubio, Quantum Electrodynamical Bloch Theory with Homogeneous Magnetic Fields, *Phys. Rev. Lett.* **123**, 047202 (2019).
- [70] V. Rokaj, Condensed Matter Systems in Cavity Quantum Electrodynamics, [arXiv:2201.01331](https://arxiv.org/abs/2201.01331) [quant-ph] (2022).
- [71] C. Ciuti, Cavity-mediated electron hopping in disordered quantum Hall systems, *Phys. Rev. B* **104**, 155307 (2021).
- [72] V. Rokaj, M. Penz, M. A. Sentef, M. Ruggenthaler, and A. Rubio, Polaritonic Hofstadter butterfly and cavity control of the quantized Hall conductance, *Phys. Rev. B* **105**, 205424 (2022).
- [73] A. Thomas, J. George, A. Shalabney, M. Dryzhakov, S. J. Varma, J. Moran, T. Chervy, X. Zhong, E. Devaux, C. Genet, J. A. Hutchison, and T. W. Ebbesen, Ground-State Chemical Reactivity under Vibrational Coupling to the Vacuum Electromagnetic Field, *Angew. Chem.* **55**, 11462 (2016).
- [74] J. Lather, P. Bhatt, A. Thomas, T. W. Ebbesen, and J. George, Cavity Catalysis by Cooperative Vibrational Strong Coupling of Reactant and Solvent Molecules, *Angew. Chem.* **58**, 10635 (2019).

- [75] A. Thomas, L. Lethuillier-Karl, K. Nagarajan, R. M. A. Vergauwe, J. George, T. Chervy, A. Shalabney, E. Devaux, C. Genet, J. Moran, and T. W. Ebbesen, Tilting a ground-state reactivity landscape by vibrational strong coupling, *Science* **363**, 615 (2019).
- [76] T. E. Li, A. Nitzan, and J. E. Subotnik, On the origin of ground-state vacuum-field catalysis: Equilibrium consideration, *J. Chem. Phys.* **152**, 234107 (2020).
- [77] J. A. Campos-Gonzalez-Angulo, Y. R. Poh, M. Du, and J. Yuen-Zhou, Swinging between shine and shadow: Theoretical advances on thermally activated vibropolaritonic chemistry, *J. Chem. Phys.* **158**, 230901 (2023).
- [78] A. Mandal, M. A. D. Taylor, B. M. Weight, E. R. Koessler, X. Li, and P. Huo, Theoretical advances in polariton chemistry and molecular cavity quantum electrodynamics, *Chem. Rev.* **123**, 9786 (2023).
- [79] J. Horak, D. Sidler, W.-M. Huang, M. Ruggenthaler, and A. Rubio, Analytic model for molecules under collective vibrational strong coupling in optical cavities, [arXiv:2401.16374](https://arxiv.org/abs/2401.16374) [[quant-ph](https://arxiv.org/abs/2401.16374)] (2024).
- [80] S. Pannir-Sivajothi, J. A. Campos-Gonzalez-Angulo, L. A. Martínez-Martínez, S. Sinha, and J. Yuen-Zhou, Driving chemical reactions with polariton condensates, *Nat. Commun.* **13**, 1645 (2022).
- [81] U. Banin, A. Bartana, S. Ruhman, and R. Kosloff, Impulsive excitation of coherent vibrational motion ground surface dynamics induced by intense short pulses, *J. Chem. Phys.* **101**, 8461 (1994).
- [82] M. Shapiro and P. Brumer, *Quantum Control of Molecular Processes* (Wiley-VCH, 2011).
- [83] C. Gerry and P. Knight, *Introductory Quantum Optics* (Cambridge University Press, Cambridge, UK, 2012).
- [84] M. Brune, F. Schmidt-Kaler, A. Maali, J. Dreyer, E. Hagley, J. M. Raimond, and S. Haroche, Quantum Rabi Oscillation: A Direct Test of Field Quantization in a Cavity, *Phys. Rev. Lett.* **76**, 1800 (1996).
- [85] A. F. Kockum, A. Miranowicz, S. De Liberato, S. Savasta, and F. Nori, Ultrastrong coupling between light and matter, *Nat. Rev. Phys.* **1**, 19 (2019).
- [86] C. K. Law and H. J. Kimble, Deterministic generation of a bit-stream of single-photon pulses, *J. Mod. Opt.* **44**, 2067 (1997).
- [87] C. L. Degen, F. Reinhard, and P. Cappellaro, Quantum sensing, *Rev. Mod. Phys.* **89**, 035002 (2017).
- [88] S. Gleyzes, S. Kuhr, C. Guerlin, J. Bernu, S. Deléglise, U. Busk Hoff, M. Brune, J.-M. Raimond, and S. Haroche, Quantum jumps of light recording the birth and death of a photon in a cavity, *Nature* **446**, 297 (2007).
- [89] A. Facon, E.-K. Dietsche, D. Grosso, S. Haroche, J.-M. Raimond, M. Brune, and S. Gleyzes, A sensitive electrometer based on a Rydberg atom in a Schrödinger-cat state, *Nature* **535**, 262 (2016).
- [90] T. Xie, Z. Zhao, X. Kong, W. Ma, M. Wang, X. Ye, P. Yu, Z. Yang, S. Xu, P. Wang, Y. Wang, F. Shi, and J. Du, Beating the standard quantum limit under ambient conditions with solid-state spins, *Sci. Adv.* **7**, eabg9204 (2021).
- [91] W.-B. Gao, C.-Y. Lu, X.-C. Yao, P. Xu, O. Gühne, A. Goebel, Y.-A. Chen, C.-Z. Peng, Z.-B. Chen, and J.-W. Pan, Experimental demonstration of a hyper-entangled ten-qubit Schrödinger cat state, *Nat. Phys.* **6**, 331 (2010).
- [92] O. Lib and Y. Bromberg, Resource-efficient photonic quantum computation with high-dimensional cluster states, *Nat. Photonics* [10.1038/s41566-024-01524-w](https://doi.org/10.1038/s41566-024-01524-w) (2024).
- [93] C. Cohen-Tannoudji, J. Dupont-Roc, and G. Grynberg, *Photons and Atoms: Introduction to Quantum Electrodynamics* (Wiley-VCH, Weinheim, Germany, 1997).
- [94] T. Busch, B.-G. Englert, K. Rzażewski, and M. Wilkens, Two cold atoms in a harmonic trap, *Foundations of Physics* **28**, 549 (1998).
- [95] C. Schäfer, M. Ruggenthaler, V. Rokaj, and A. Rubio, Relevance of the quadratic diamagnetic and self-polarization terms in cavity quantum electrodynamics, *ACS Photonics* **7**, 975 (2020).
- [96] R. Shankar, *Principles of Quantum Mechanics*, 2nd ed. (Springer, 1994).
- [97] D. Tannor, *Introduction to Quantum Mechanics: A Time-Dependent Perspective*, 1st ed. (University Science Books, 2007).
- [98] L. Mandel, Sub-Poissonian photon statistics in resonance fluorescence, *Opt. Lett.* **4**, 205 (1979).
- [99] D. M. Welakuh, M. Ruggenthaler, M.-L. M. Tchenkoue, H. Appel, and A. Rubio, Down-conversion processes in *ab initio* nonrelativistic quantum electrodynamics, *Phys. Rev. Research* **3**, 033067 (2021).
- [100] D. F. Walls and G. J. Milburn, *Quantum Optics* (Springer Berlin, Heidelberg, 2008).
- [101] G. Rempe, R. J. Thompson, R. J. Brecha, W. D. Lee, and H. J. Kimble, Optical bistability and photon statistics in cavity quantum electrodynamics, *Phys. Rev. Lett.* **67**, 1727 (1991).
- [102] C. W. Gardiner and M. J. Collett, Input and output in damped quantum systems: Quantum stochastic differential equations and the master equation, *Phys. Rev. A* **31**, 3761 (1985).